POLITECNICO
MILANO 1863

SCUOLA DI INGEGNERIA INDUSTRIALE
E DELL'INFORMAZIONE

Development of a Comprehensive Technology Database for the design optimization of Aggregated Energy Systems with My-AESOPT

TESI MAGISTRALE IN ENERGY ENGINEERING – GREEN POWER SYSTEM (EEG)

Puddu, Mattia, 252036

Advisor:
Prof. Emanuele Martelli

Co-advisors:
Dott. Vincenzo Dipierro

Academic year:
2024-25

Abstract: This thesis presents the development of a comprehensive technology database containing detailed economic and technical data for energy technologies that can be adopted within an Aggregated Energy System (AES). The database is specifically designed to serve as input for the design optimization of AESs (microgrids, Multi energy systems, virtual power plants, etc.) through My-AESOPT.

My-AESOPT is a comprehensive multi-year optimization tool for optimal investment planning of Aggregated Energy Systems, developed by the research group of Prof. Martelli at Politecnico di Milano. It is formulated as a Mixed-Integer Linear Programming (MILP) model and is capable of accounting for multiple investment stages over the planning horizon. The tool performs a detailed hourly optimization of AES operation, explicitly considering the technical characteristics of installed technologies: part-load performance modeling, size effects, and other relevant operational parameters, ensuring reliable and accurate results.

The developed database is then applied to a case study representative of a hospital located in Northern Italy. The objective is to demonstrate both the effectiveness of My-AESOPT in identifying economically and environmentally optimal configurations and the reliability of the implemented input data. The results show that significant reductions in CO_2 emissions (47.6%) can be achieved with only a limited increase in Net Present Cost (NPC) (6.5%) compared to a reference configuration, highlighting the potential of My-AESOPT to support cost-effective decarbonization strategies in AES.

Key-words: Aggregated Energy Systems, My-AESOPT, Technology Database, optimization,

1. Introduction

There is an undeniable link between urban development, quality of life, and energy consumption. However, in light of the growing urgency of climate change, the increase in energy production must be accompanied by a transition toward cleaner systems that are less dependent on fossil fuels, with greater emphasis on energy efficiency and electrification. Although the pursuit of these objectives significantly increases system complexity, several complementary and non-mutually exclusive solutions have been proposed.

Among these solutions, the approach central to this thesis is that of Aggregated Energy Systems (AESs). The term AES covers a broad class of integrated energy configurations, including District Energy Systems (DESs), Multi-Energy Systems (MESs), as well as microgrids and Virtual Power Plants (VPPs). Broadly defined, an Aggregated Energy System (AES) constitutes a framework where diverse energy demands, technologies and vectors are integrated and simultaneously optimized.

To better understand the concept of AESs, it is useful to first examine the defining characteristics of District Energy Systems, which represent one of their most relevant and well-known implementations.

District Energy Systems represent fundamental building blocks of the Smart Energy System paradigm. Through the integration of multiple energy vectors, diversified energy and heat production technologies (including renewable sources), and energy storage solutions, these systems are expected to play a crucial role in achieving decarbonization and sustainability targets.

In simplified terms, a DES can be described as a coordinated aggregation of multiple energy and/or heat demands, while, from an urban perspective, it consists of a group of buildings or urban units with different energy requirements. These requirements depend on several factors, including building size, function, seasonal variations, and the behavioral patterns of occupants. Moreover, DESs can benefit from interconnections both with other district systems and with the main electricity grid. These connections enable interaction and cooperation, improving overall system performance compared to traditional isolated approaches. At the same time, grid integration allows bidirectional electricity exchange, enhancing operational flexibility.

As discussed by Mancarella [1], Multi-Energy Systems are considered a key enabler of the transition toward a cleaner energy future: their importance lies in their ability to integrate renewable energy sources, increase energy conversion efficiency, and enhance overall system flexibility through the coordinated use of multiple energy vectors.

While the advantages of Aggregated Energy Systems are numerous, they come at the cost of increased system complexity, particularly during the design and planning phases. The integration of multiple technologies, energy vectors, and operational strategies significantly increases the possible solutions which have to be considered for identifying the optimal configuration, making traditional design approaches inadequate. For this reason, several optimization models have been developed to support system planning and operation under such complexity.

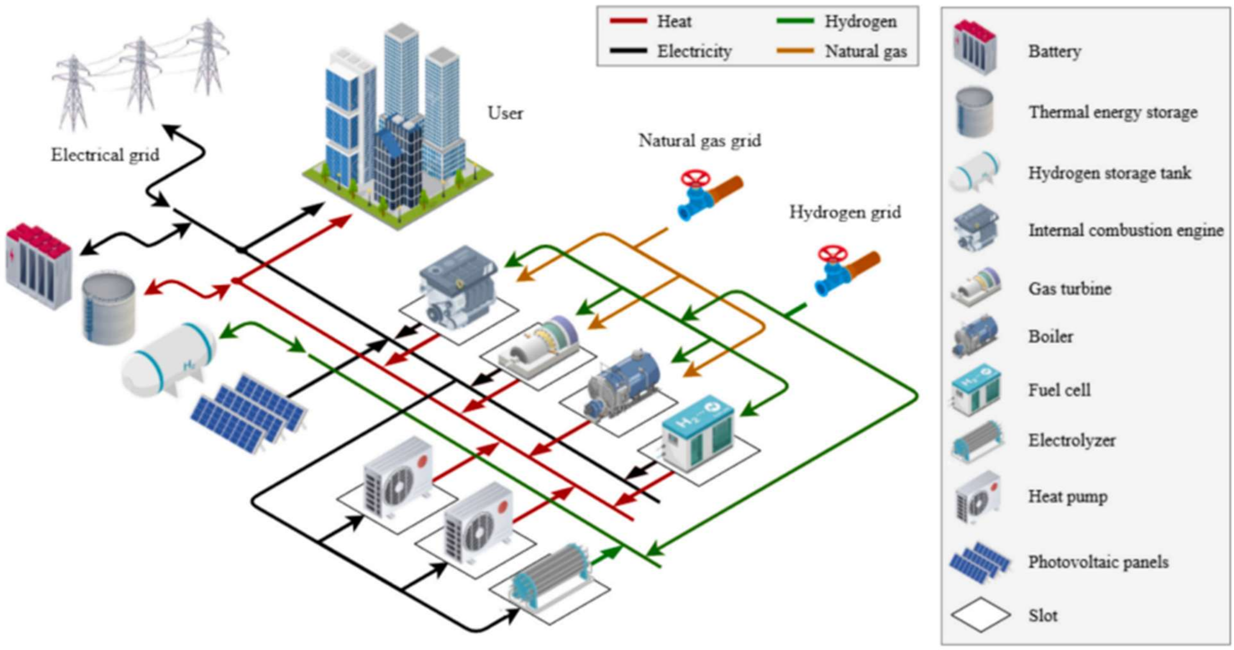

Figure 1: Schematical representation of the slot-based structure of AES.

This thesis focuses in particular on My-AESOPT, the tool proposed by Dipierro et al. [2], for the optimal investment planning of Aggregated Energy Systems (an example of AES is presented in Figure 1). My-AESOPT is based on a Mixed-Integer Linear Programming (MILP) model, and the tool is designed to perform multi-step design optimization, allowing detailed and accurate representation of AES configurations in both the investment planning and operational phases.

However, the reliability and validity of the results produced by My-AESOPT are strongly dependent on the quality of the input data. Accurate, representative, and up-to-date technical and economic parameters are essential to ensure that optimization results reflect realistic market conditions.

In this context, the present thesis contributes by conducting a comprehensive research and analysis of the current state of the energy technologies market. The work systematically collects and organizes both technical and economic data for a wide range of energy conversion and storage technologies suitable for AES applications. Particular emphasis is placed on producers' data, which are considered especially valuable in ensuring that the optimization results remain consistent with real-world technological and economic conditions.

Given the rapid evolution of the energy sector, another goal of this thesis is to identify not only the most reliable data available, but also recent, thereby guaranteeing the relevance, in the future years, of the developed database. In cases where manufacturers' data, particularly economic data, were not publicly accessible, reputable academic sources were used to fill the gaps: by adopting this strategy, the reliability of the data is preserved without compromising the completeness of the dataset necessary for the optimization model.

Consequently, this thesis aims to provide a structured and reliable database to be used as input for My-AESOPT in the optimal investment planning of Aggregated Energy Systems. At the same time, it serves as a reference framework that can reduce the research effort required to gather input data and support validation/comparison of other resources.

The resulting database is structured in two complementary formats. The first format presents technical and economic data for fixed system sizes, directly derived from manufacturers' specifications or academic sources. The second format adjusts and reworks these data to determine best-fit correlations (compatible with My-AESOPT MILP model) valid for energy systems with variable sizes. In this case, the original data have been reformulated to allow users to estimate the relevant technical and economic parameters across a defined capacity range: this approach preserves consistency with real-world conditions while providing greater flexibility for optimization and scenario analysis.

2. Description of My-AESOPT

My-AESOPT is a comprehensive multi-year optimization tool for the optimal investment planning of Aggregated Energy Systems (AESs): developed at the Energy Department of Politecnico di Milano, it is presented in the work by Dipierro et al. [2]. The tool is formulated as a Mixed-Integer Linear Programming (MILP) model and is capable of taking into account multiple investment stages over the planning horizon. In addition to long-term investment decisions, My-AESOPT performs a detailed hourly optimization of AES operation, explicitly considering the technical characteristics of the installed technologies.

As discussed previously, understanding the structure and functioning of Aggregated Energy Systems is essential to fully grasp how My-AESOPT operates. AESs can integrate multiple technological solutions and supply different energy vectors, such as electricity and heat. More importantly, they can exploit synergies arising from the coordinated use of multiple energy carriers and conversion technologies: these synergies enhance not only energy performance and overall efficiency, but also economic performance and operational flexibility.

However, these advantages are accompanied by increased complexity, particularly during the design phase. For example, energy units do not necessarily operate at nominal capacity during real operation; therefore, their partial-load performance must be properly contemplated already at the planning stage. Additional complexity arises from the simultaneous management of multiple energy vectors, especially those directly linked to end-user demand. Consequently, the energy flows among technologies and demand nodes must be carefully modelled and optimized during the design phase to ensure technical feasibility, economic viability, and effective system integration, while also guaranteeing sufficient flexibility of the whole energy system.

My-AESOPT represents one of the advanced tools that can effectively support the design phase of Aggregated Energy Systems by optimizing the case study configuration while accounting for the various technical, economic, and operational constraints discussed above. The main features of My-AESOPT can be summarized as follows:

- **Multi-stage investment planning.**
  The tool enables the modeling of AES development over a multi-year horizon, allowing for multiple investment stages during which energy units can be installed, replaced, or decommissioned. It supports both fixed-size and continuous-size technologies, as well as modular and non-modular units. This flexibility allows the user to represent and take into consideration the temporal evolution of the system configuration when multiple investment steps are applied.

- **Slot-based installation constraints.**
  The number of units that can be installed is regulated through a slot-based system, which accounts for spatial limitations and physical installation constraints. This feature ensures that the optimization results remain feasible and consistent with practical requirements.

- **Detailed operational modeling.**
  My-AESOPT performs hourly operational optimization of all installed technologies. For dispatchable units, both nominal and part-load performance are accurately represented. The model includes key technical constraints (such as ramp-up and ramp-down limits, start-up processes, shut-down processes, and other operational restrictions) necessary to realistically simulate the behavior of the system's energy units. In addition, the tool supports the modelling of cogeneration, co-firing, and the use of multiple energy vectors and fuels; in particular, in the case of co-firing, the model is also capable of optimizing the fuel mix.

- **Reliability constraints.**
  The model incorporates reliability analysis to ensure that energy demands are met even in the event of failure of one or more operating units: this feature strongly enhances the robustness of the optimal design.

- **Flexibility and applicability.**
  My-AESOPT is designed to guarantee ease of use and be adaptable to a wide range of case studies. It can accommodate different AES configurations, as well as case-specific constraints and technical characteristics, making it a versatile tool for investment planning and system analysis.

Thanks to these and other advanced functionalities, My-AESOPT ensures a high level of accuracy and detail in the optimization of Aggregated Energy Systems. To assess its effectiveness in realistic scenarios, the tool was validated through multiple case studies presented by Dipierro et al. [2]. The results demonstrate a high degree of accuracy, together with significant reductions in CO_2 emissions and only a limited increase (below 20%) in investment costs compared to the reference design solution: these findings also highlight the potential role of My-AESOPT as a strategic tool in supporting decarbonization pathways.

Alternatively, the tool can be employed with a primary focus on cost minimization. The results reported by Dipierro et al. [2] show that the optimized and reliability-constrained AES configuration achieved investment cost savings of up to 39% compared to a non-optimized reference design.

In addition, My-AESOPT can be employed for sensitivity analyses, enabling the evaluation of the impact of variations in key parameters such as fuel prices, incentive schemes, carbon taxation, and other economic or regulatory factors. This capability further enhances its value as a decision-support tool for long-term strategic planning under uncertainty, allowing the assessment of specific scenarios such as increases in fossil fuel prices, changes in incentives, or the introduction/adjustment of carbon taxes.

3. Characteristics of Technology Databases

As discussed previously, the primary objective of this thesis is to develop a comprehensive database of technical and economic data for energy technologies that can be incorporated into the design of an Aggregated Energy System (AES). This fixed-size database enables My-AESOPT to evaluate a wide range of alternatives during the optimization process and identify the most suitable configuration for a given case study. Also, in the context of the optimization of AES, the availability of a variable-size database along the already introduced fixed-size database is crucial, as it enables the optimizer to treat the size of each energy unit as a decision variable rather than a fixed parameter.

Although the databases include an extensive number of energy technologies, they can be classified into three main categories:

- **Dispatchable units:** these are energy technologies whose power output can be actively controlled, started, stopped, increased, or decreased, according to system requirements and within the technical constraints defined by their operational characteristics.
- **Non-dispatchable units:** these energy technologies have outputs that are primarily determined by uncontrollable factors, such as meteorological or environmental conditions. Their generation cannot be scheduled or adjusted to demand (except through curtailment) and must generally be balanced by other components within the energy system.
- **Energy storage units:** these technologies absorb energy at one point in time, store it in a physical or chemical form, and release it at a later time as electricity or another usable energy carrier. Their primary advantage lies in enabling temporal energy shifting, which enhances overall system flexibility, particularly in systems that include non-dispatchable energy sources.

The vast majority, but not all, energy technologies potentially installable in an AES have been examined in this thesis. For certain technologies, such as air-to-air heat pumps, the available data was either inconclusive or deemed insufficiently reliable to be included in the databases. For other technologies, external simulation tools can be employed to obtain performance and economic results. One such tool is Thermoflex, which allows the modular assembly of multiple system components and the simulation of energy and mass balances under both on-design and off-design operating conditions.

The energy technologies analyzed in this thesis, classified according to the categories introduced previously, are as follows:

- **Dispatchable units:** ICE CHP (internal combustion engines with cogeneration), SOFC CHP (solid oxide fuel cells with cogeneration), PEMFC CHP (proton exchange membrane fuel cells with cogeneration), natural gas condensing and non-condensing boilers, air–water heat pumps, large water–water heat pumps, geothermal heat pumps (using groundwater wells, borehole probes, or horizontal collectors), large alkaline electrolyzers, large PEM electrolyzers, wood chip boilers, pellet boilers, biomass ORCs (organic Rankine cycles), large absorption chillers (with water or high-pressure steam as the heat source), large compression chillers and large absorption chillers.
- **Non-dispatchable units:** monocrystalline PV panels, vertical-axis wind turbines (VAWTs), horizontal-axis wind turbines (HAWTs) at both utility and distributed scales, solar thermal panels (roof-mounted or open-air systems), and concentrated solar power (CSP) installations.
- **Energy storage units:** battery energy storage systems (BESSs), large thermal energy storage systems (TESs), hydrogen storage tanks, and hydrogen storage caverns.

It is worth mentioning that, for heat pumps, the data were derived from models capable of providing both heating and cooling. This dual functionality enhances the operational flexibility of these units and, by extension, of the overall energy system in which they are integrated.

Finally, the content of the database, initially referring to the fixed-size alternatives, will be presented for each of the three categories in the following sections.

3.1 Dispatchable Technologies

For dispatchable energy technologies, the database includes:

- **Technical data:** this includes unit size, input and output power at both minimum partial load and nominal operating points, hot ramp-up and ramp-down rates, start-up and shut-down times, fuel type, and lifetime. All sources and references used to obtain this data are also documented.
- **Economic data:** this includes capital expenditure (CAPEX), variable operation and maintenance (O&M) costs, variable O&M costs including replacements, fixed O&M costs, and start-up costs. All sources and references used to obtain this data are also documented.

While My-AESOPT primarily requires data expressed in terms of the energy input to each unit, the database provides both input- and output-referred data. This ensures compatibility with external studies or tools that may prefer output-based parameters: unit size, CAPEX, all O&M costs and start-up costs are referred to both input and output.

3.2 Non-Dispatchable Technologies

For non-dispatchable energy technologies, the database includes:

- **Technical data:** this includes unit size, hot ramp-up and ramp-down rates, start-up and shut-down times, fuel type, and lifetime. All sources and references used to obtain this data are also documented.
- **Economic data:** this includes capital expenditure (CAPEX), variable operation and maintenance (O&M) costs, variable O&M costs including replacements, fixed O&M costs, and start-up costs. All sources and references used to obtain this data are also documented.

3.3 Energy Storage Units

For energy storage technologies, the database includes:

- **Technical data:** this includes unit size, C-rate, indications on the ramp-up, on the ramp-down, on the start-up time and shut-down time, and lifetime**.** All sources and references used to obtain this data are also documented.
- **Economic data:** this includes capital expenditure (CAPEX), variable operation and maintenance (O&M) costs, variable O&M costs including replacements, fixed O&M costs, and start-up costs. All sources and references used to obtain this data are also documented.

3.4 Explanations of Technical Data

For clarity, some of the technical parameters included in the database are defined as follows:

- **Ramp-up:** The rate at which a generating unit can increase its power output, expressed as a percentage of rated capacity per minute.
- **Ramp-down:** The rate at which a generating unit can decrease its power output, expressed as a percentage of rated capacity per minute.
- **Start-up time:** The time required for an energy unit to transition from an offline state to its minimum stable operating point.
- **Shut-down time:** The time required for an energy unit to transition from its operating point to an offline state.

- **C-rate:** For battery storage systems, the C-rate indicates the speed at which the battery can charge or discharge relative to its total energy capacity. It is calculated as the ratio of power to energy capacity and expressed in per hours (h^{-1}).

3.5 Final Considerations on Database Structure

The technical and economic data described above refer to the fixed-size database. For the variable-size database, several modifications have been introduced to allow more flexible and accurate modelling:

1. **Size range:** Instead of a single fixed size, each energy unit is represented by a range of possible sizes.
2. **Part-load coefficients:** A set of coefficients (k_1, k_2, k_3 for each output) is included to accurately model part-load operation of energy units across the size range.
3. **Normalized power values:** Input and output power at minimum and nominal operating points are expressed as ratios relative to the unit's nominal input size, ensuring consistency across different sizes.
4. **CAPEX correlations**: instead of the specific CAPEX, for each energy technology, and for each of its size ranges, a CAPEX correlation is presented.

4. CAPEX correlations

Although this thesis provides several discrete data points for each energy technology, including the corresponding economic parameters, users may wish to analyze systems with sizes that differ from those explicitly included in the fixed-size database. Since most economic parameters are directly linked to capital expenditure, it is essential to derive specific CAPEX correlation functions that allow the estimation of specific investment costs (€/kW) as a function of system size.

This additional modeling step enhances flexibility, granting users greater freedom in selecting the size and configuration of the energy technologies to be provided as input to My-AESOPT. While the use of cost correlations may introduce a limited reduction in accuracy compared to discrete manufacturer data, this drawback is mitigated by the validation tools built-in the developed script. These tools enable users to assess whether the fitted correlation adequately represents the original data points and remains sufficiently accurate within the defined range: the results that were obtained maintain a coefficient of determination R^2, which is always higher than 0.95.

To derive the specific CAPEX correlations, real data obtained from manufacturers, or, when unavailable, from academic sources, at fixed sizes are provided as input to a dedicated script: the same data that populates the fixed-size database was used for this purpose. The script returns a functional correlation that can be used to estimate CAPEX values for any system size within the applicable range.

Two different fitting approaches are implemented and compared, as the performance of each method may vary depending on the characteristics and distribution of the input data:

- **Log–log linear regression**, typically used when cost–capacity relationships closely follow a power-law behavior.
- **Non-linear curve fitting**, which can give better results when deviations from simple scaling laws are observed.

The results obtained from both methods are compared against the original data points, and the most appropriate correlation is selected based on goodness-of-fit criteria and consistency with known cost points. Both methods are implemented in the script provided in Appendix A, and the most relevant sections will be analyzed in the following paragraphs to clarify their structure and functionality.

In the first section of the script, the empirical data must be provided as input. The array **x** contains the fixed system sizes, while the array **y**, which must have the same length as **x**, contains the corresponding specific investment costs associated with those sizes. As previously discussed, the unit of **y** is €/kW (or €/MW for large energy units), since it represents the specific CAPEX, while the unit of **x** is kW.

In the present work, the input data corresponds to the values included in the fixed-size database. However, users may easily extend or replace these data points with additional size and cost pairs derived from their own research, at the possible expense of only a marginal increase in computational time.

The correlation adopted for CAPEX estimation follows a power-law formulation, which is common to all the technologies analyzed:

$$y = a \cdot x^b$$

where a and b are parameters determined by the fitting procedure. Since, for all technologies considered, the specific CAPEX decreases as system size increases, the exponent b is always negative. For clarity, the model is therefore reformulated as:

$$y = a \cdot x^{-k} \text{ with } k > 0$$

where k represents the positive scaling exponent returned by the script together with the coefficient a.

To better understand the practical role of these parameters, it is useful to briefly examine their influence on the value of y. The coefficient a primarily affects the cost level at smaller sizes: higher values of a result in higher specific CAPEX for small-scale systems, although its relative influence diminishes as system size increases. Conversely, the scaling exponent k governs the rate at which specific CAPEX decreases with size. Larger values of k imply a steeper cost reduction for small-to-medium sizes, while the marginal decrease in y becomes progressively less pronounced as x increases.

This behavior reflects the well-known economies-of-scale effect typically observed in energy technologies.

In the second section of the script, the first fitting approach is implemented: a log–log linear regression performed using the **linregress** function. This method computes a linear least-squares regression between two sets of measurements and is applied to the logarithmic transformation of the variables. Specifically, by taking the logarithm of both sides of the power-law model

$$y = a \cdot x^{-k}$$

the equation becomes linear in logarithmic space:

$$\log(y) = \log(a) - k\log(x)$$

This transformation enables the estimation of the parameters through linear regression, where the intercept corresponds to $\log(a)$and the slope corresponds to $-k$.

Log–log linear regression is intentionally applied before the non-linear fitting procedure for a critical reason: the non-linear fit requires an initial parameter guess to ensure convergence. The parameter estimates obtained from **linregress** provide reliable initial values for *a* and *k*, thereby improving the stability of the subsequent non-linear optimization.

After performing the regression, the script outputs the estimated parameters along with the coefficient of determination (R^2). This indicator provides an initial quantitative assessment of how accurately the fitted curve approximates the input data and, consequently, how well the derived correlation represents the observed cost–size relationship. In other words, R^2 explains variance and how well the model captures trends.

The second fitting approach implemented in the script is a non-linear regression performed using the **curve_fit** function. Unlike the previous method, this procedure operates directly in linear space and applies non-linear least squares to fit the selected power-law model to the original data.

As previously mentioned, the non-linear fitting process is initialized using the parameter estimates obtained from the log–log linear regression (**linregress**). Providing these initial guesses for the parameters improves convergence stability and reduces the risk of the algorithm converging to non-physical or suboptimal solutions.

It is important to note that neither method is universally superior. The quality of the fit strongly depends on the characteristics of the input data. In general, the non-linear fitting approach tends to perform better when the dataset contains noise or when smaller system sizes play a significant role in the correlation. Conversely, log–log linear regression often provides more stable and accurate results when the input data exhibit limited noise and may offer better extrapolation behavior for larger system sizes.

After performing the non-linear regression, the script outputs the estimated parameters together with their associated uncertainties. These uncertainties provide an indicator of parameter reliability and play a role analogous to the coefficient of determination (R^2) reported for the log–log regression, offering a quantitative measure of the goodness and robustness of the fit, also allowing comparison between the two possible results.

The final section of the script, which is available in Appendix A, is dedicated to the graphical comparison of the fitted CAPEX correlations against the original data points, which consists in the main diagnostic tool of the script.

First, a dense array of size values is generated within the range of the input dataset. Using this array, the corresponding predicted specific CAPEX values are computed for both fitting methods (log–log linear regression and non-linear fit). This step ensures that the fitted curves are represented as smooth and continuous functions when plotted.

Two complementary plots are then produced:

1. **Log–log plot: i**n this plot, both axes are expressed on a logarithmic scale. This representation is particularly useful because the adopted model follows a power-law relationship. In log–log space, a power-law function appears approximately linear, making it easier to visually control the consistency of the scaling behavior, notice deviations from linearity, and compare the quality of the two fitting methods.
2. **Linear-scale plot: t**he second plot displays the same data and fitted curves on standard linear axes. This visualization provides a more intuitive understanding of how the estimated

specific CAPEX varies with system size in absolute terms. It is especially useful for evaluating the deviations between the fitted curves and the original data.

By combining these two graphical representations, which serve primarily as a diagnostic tool, the script provides a qualitative validation of the fitting results, complementing the coefficient of determination (R^2). These two systems enhance confidence in the selected CAPEX correlation before it is adopted in the database.

5. Linearization of performance maps

In the variable-size sheet of the database, a set of coefficients (k_1, k_2, k_3) is provided for each applicable technology (or multiple sets where multiple size ranges are present for a single energy technology), which correspond to the linearized performance maps. These coefficients are introduced to accurately represent the part-load operation of energy units while maintaining a reasonable level of model simplicity and computational efficiency.

The adopted formulation is based on the part-load model originally proposed by Lahdelma and Hakonen [3], combined with the operational strategy introduced by Yokoyama et al. [4]. The latter approach has been slightly modified to enable linearization of size-dependent effects on both capital costs and performance parameters, and this methodology has been extensively analyzed and applied by Zatti [5] in the context of part-load modeling for energy units within Aggregated Energy Systems.

The approach relies on a key assumption: the nominal size of an energy unit can be treated as a continuous decision parameter. This assumption is justified by the wide range of commercially available technologies, which ensures that, in practical applications, a unit with a size very close (or equivalent) to the one determined by My-AESOPT can typically be identified on the market.

The modeling of size effects and part-load performance for energy conversion units is therefore based on the coefficient set (k_1, k_2, k_3). These coefficients are determined through regression procedures and are subsequently used to linearize both the input (e.g., fuel consumption) and the useful outputs of the unit, such as, in the case of cogeneration technologies, both thermal and electrical power.

The equations presented below, which describe the relationship between input energy and multiple outputs for an internal combustion engine operating in cogeneration mode, highlight the central role of the three coefficients. Accurate determination of these parameters is essential to ensure that the simplified linearized model reliably captures the real performance characteristics of the technology across different sizes and load levels.

Although the example refers to an internal combustion engine with cogeneration, the same methodological framework can be applied to any energy unit. The only required adaptation consists of redefining the nature of the input and output variables according to the specific technology under consideration.

The methodology introduced by Zatti [5] has been slightly adapted (1) to meet the objectives of this thesis. For a cogeneration technology, which simultaneously produces both electricity and heat, the two outputs can be represented using linearized equations as follows:

$$\begin{cases} P_{EE} = k_{1,EE} \cdot INPUT + k_{2,EE} \cdot XD_{EE} + k_{3,EE} & (1a) \\ P_{TH} = k_{1,TH} \cdot INPUT + k_{2,TH} \cdot XD_{TH} + k_{3,TH} & (1b) \end{cases}$$

where:

- $k_{1,EE}$, $k_{2,EE}$, $k_{3,EE}$ are the linear coefficients used to compute the electrical output as a function of fuel input and the unit size.
- $k_{1,TH}$, $k_{2,TH}$, $k_{3,TH}$ are the linear coefficients used to compute the thermal output as a function of fuel input and the unit size.
- INPUT represents the fuel consumed by the cogeneration unit, measured in kW.
- P_{EE} is the electrical power output of the cogeneration unit, measured in kW.
- P_{TH} is the thermal power output of the cogeneration unit, measured in kW.
- XD_{EE} and XD_{TH} are the nominal sizes of the cogeneration unit (referred respectively to electricity and heat), measured in kW.

These equations also illustrate why two separate sets of coefficients are required for cogeneration technologies, one for the electrical output and another for the thermal output. In contrast, for energy technologies that produce a single type of output (not necessarily heat or electricity, this can be applied also to cooling, hydrogen electrolysis and more), only one set of coefficients and a single equation are necessary to model the input–output relationship accurately.

By employing this linearized approach, it is possible to portray the part-load performance (which is controlled by the parameter INPUT) of the cogeneration unit while incorporating the influence of unit size, enabling My-AESOPT to optimize both design and operation accurately.

The importance of the previously introduced equations and coefficient sets, as highlighted by Zatti [5], can be demonstrated by deriving the efficiency of a cogeneration unit directly from the input–output relationships.

The electrical efficiency (η_{EE}) of the cogeneration unit can be expressed as the ratio of electrical power output to fuel input (2):

$$\eta_{EE} = \frac{P_{EE}}{INPUT} = k_{1,EE} + k_{2,EE} \cdot \frac{XD_{EE}}{INPUT} + \frac{k_{3,EE}}{INPUT} \qquad (2)$$

where η_{EE} represents the electrical efficiency of the unit, P_{EE} is the electrical output, INPUT is the fuel consumed, XD_{EE} is the nominal electrical size of the unit, and $k_{1,EE}$, $k_{2,EE}$, $k_{3,EE}$ are the previously defined linear coefficients.

Similarly, the thermal efficiency (η_{TH}) can be calculated as the ratio of thermal power output to fuel input (3):

$$\eta_{TH} = \frac{Q_{TH}}{INPUT} = k_{1,TH} + k_{2,TH} \cdot \frac{XD_{TH}}{INPUT} + \frac{k_{3,TH}}{INPUT} \qquad (3)$$

where η_{TH} represents the thermal efficiency of the cogeneration unit, P_{TH} is the thermal output, and $k_{1,TH}$, $k_{2,TH}$, $k_{3,TH}$ are the corresponding coefficients.

These expressions clearly demonstrate how the linear coefficient sets not only allow the estimation of output power at various part-load conditions but also enable the straightforward calculation of the electrical and thermal efficiencies as functions of fuel input and unit size. This capability is essential for accurately capturing part-load performance in My-AESOPT and for evaluating the operational effectiveness of AES technologies under varying load and size conditions.

To further emphasize the role of the coefficient sets, it is useful to interpret the physical meaning of each parameter:

- k_1 can be regarded as the "constant" efficiency of the energy unit, representing the performance if dependencies on both load and size were neglected.
- k_2 captures the variation of efficiency with part-load operation, reflecting how the unit's performance changes when operating below nominal capacity.
- k_3 represents the effect of unit size on efficiency, accounting for size-dependent performance characteristics.

The coefficient sets were determined using the least-squares method, applied to the input and output data of detailed energy unit models under both nominal and minimum (part-load) operating conditions, while making sure that P_{EE} and P_{TH} obtained with sets of coefficients do not introduce an error higher than 5% (with respect to the known points).

In summary, correctly obtaining these sets of coefficients is critical for accurately modeling the part-load performance of variable-size units, since proper representation of part-load behavior is fundamental in describing the operational characteristics of energy units within an Aggregated Energy System (AES), ensuring that My-AESOPT can optimize both design and operation in a realistic and accurate manner.

6. Fixed-size and Variable-size databases

Due to the extensive amount of information contained in the databases, their complete versions are reported in Appendix A, where all the technical and economic parameters (for the technologies considered are fully documented), along all the references for the presented values.

For transparency and reproducibility, it is essential to explicitly report the sources of the main economic and performance data included in the database.

Table 1: References for performance and economic parameters.

Energy Technology	Size range	Reference CAPEX	Reference OPEX	Reference performance
ICE CHP	2 - 10000 kW_{el}	[6]	[6]	[7]
SOFC CHP	1.5 - 1000 kW_{el}	[8]	[9]	[10]
PEM FC CHP	5 - 500 kW_{el}	[11]	[12]	[13]

NG boiler condensing	10 - 500 kW_{th}	[6]	[6]	[14]
NG boiler non-condensing	0.5 - 30 MW_{th}	[6]	[6]	[15]
Heat pump (air - water)	5 - 20000 kW_{th}	[6]	[6], [16]	[17]
Heat pump (water-water) (large)	1 - 50 MW_{th}	[6]	[6], [16]	[17]
Geo Water-Water Heat Pump	5 – 1000 kW_{th}	[6]	[6], [18]	[17]
Alkaline electrolyzer (large)	1-20 MW_{el} (input)	[19]	[20]	[21]
PEM electrolyzer (large)	1-20 MW_{el} (input)	[19]	[20]	[22]
Wood Chip Boiler	20 - 1500 kW_{th}	[6]	[6], [23]	[24]
Pellet Boiler	10 - 150 kW_{th}	[6]	[6], [23]	[24]
Biomass ORC	1 – 10 MW_{th}	[25]	[26]	[27]
Absorption chiller (water)	1000 - 10000 kW_{th}	[28]	[29], [28]	[30]
Absorption chiller (steam)	1000 - 20000 kW_{th}	[28]	[29], [28]	[31]
Compression chiller (large)	50 - 10000 kW_{th}	[32]	[33]	[17]
PV panels	2.5 kW_{el} - 100 MW_{el}	[34], [35]	[36], [37], [35]	[35]
Wind Turbines – Utility scale	2 - 200 MW_{el}	[38], [35]	[38], [10], [35]	[35]
Wind Turbine – Distributed	2.5 - 1500 kW_{el}	[36]	[38], [36], [10], [35]	[36]
Solar Thermal (roof system)	5 -140 kW_{th}	[6]	[6], [10]	[6]
Solar Thermal (open-air system)	140 - 10500 kW_{th}	[6]	[6], [10]	[6]

Concentrated solar thermal	50 – 250 MW_{el}	[39]	[36]	[39], [35]
BESS (battery energy storage system)	3 kW_{el} - 100 MW_{el}	[36]	[40], [36]	[36]
TES (thermal energy storage)	10 – 3000 MWh	[41]	[40]	[41], [42]
Hydrogen storage tank	10 – 10000 kg_{H2}	[43]	[40]	[43]
Hydrogen storage cavern	1000 - 50000 ton_{H2}	[44], [8]	[40]	[44]

6.1 CAPEX correlations results

The script introduced in Section 4 produced, as output, the CAPEX scaling correlations derived for the analyzed energy technologies. These correlations, expressed in the form of a power-law function $y = a \cdot x^{-k}$, represent the relationship between the nominal size of the technology and its specific investment cost.

The resulting values of the parameters a and k, obtained through the method described previously, are summarized in Table 2 and are implemented in the variable-size database to easily obtain economic input data for My-AESOPT.

Table 2: CAPEX correlations

Energy unit	CAPEX correlations
ICE CHP	$y = 18729.721 * x^{(-0.401)}$ *(till 0.5 MW_el)* $y = 1908.689 * x^{(-0.065)}$ *(till 10 MW_el)*
SOFC CHP	$y = 21292.176 * x^{(-0.224)}$
PEMFC CHP	$y = 18263.477 * x^{(-0.205)}$
NG BOILER Condensing (small)	$y = 4634.174 * x^{(-0.541)}$
NG BOILER Non-Condensing (large)	$y = 113.393 * x^{(-0.280)}$
Heat pump (air-water) Heating	$y = 4036.605 * x^{(-0.182)}$
Heat pump (air-water) Cooling	$y = 3966.302 * x^{(-0.182)}$

Heat pump large/industrial (water-water) Heating	$y = 71318.451 * x^{(-0.455)}$
Heat pump large/industrial (water-water) Cooling	$y = 72712.965 * x^{(-0.455)}$
Geo Water-Water Heat Pump (Groundwater Well) Heating	$y = 6583.713 * x^{(-0.257)}$
Geo Brine–Water Heat Pump (Borehole probes) Heating	$y = 8428.941 * x^{(-0.249)}$
Geo Brine–Water heat pump (Collectors) Heating	$y = 7148.334 * x^{(-0.244)}$
Geo Water-Water Heat Pump (Groundwater Well) Cooling	$y = 6836.872 * x^{(-0.257)}$
Geo Brine–Water Heat Pump (Borehole probes) Cooling	$y = 8742.778 * x^{(-0.249)}$
Geo Brine–Water heat pump (Collectors) Cooling	$y = 7409.049 * x^{(-0.244)}$
Wood Chip Boiler	$y = 2554.662 * x^{(-0.372)}$
Pellet Boiler	$y = 2932.798 * x^{(-0.494)}$
Biomass ORC	$y = 6011.595 * x^{(-0.601)}$
Absorption chiller large (heat source: steam high pressure)	$y = 4122.933 * x^{(-0.223)}$
PV monocrystalline	$y = 5142.023 * x^{(-0.162)}$
Wind Turbine Utility (Hor. Axis)	$y = 2285.007 * x^{(-0.101)}$
Wind Turbine Distributed (Hor. Axis)	$y = 13709.991 * x^{(-0.211)}$
Solar thermal hot water (roof system)	$y = 3765.421 * x^{(-0.320)}$
Solar thermal hot water (open-air systems)	$y = 861.516 * x^{(-0.079)}$
Solar thermal hot water (general)	$y = 2748.712 * x^{(-0.227)}$
BESS (Crate = 1/4)	$y = 5177.631 * x^{(-0.092)}$

As previously explained, the variable y represents the specific investment cost, expressed in €/kW, while x denotes the nominal size of the technology in kW. The only exceptions are non-condensing natural gas boilers, utility-scale wind turbines, and biomass Organic Rankine Cycle (ORC) systems, for which y is expressed in €/MW and x in MW.

For some energy technologies, however, the data available from manufacturers and academic literature were not sufficient, either in quantity or in consistency, to derive a reliable power-law scaling correlation. In such cases, fitting a regression model would have introduced excessive uncertainty and, possibly, misleading results.

Therefore, for these specific technologies, the CAPEX has been implemented as a constant specific investment cost, independent of size, once again from producers from reputable academic sources. The adopted constant values are reported in Table 3.

Table 3: Constant specific CAPEX

Energy unit	Specific CAPEX
Alkaline electrolyzer	2330 €/kW_{el}
PEM electrolyzer	3250 €/kW_{el}
Absorption chiller large (heat source: hot water)	1500 €/kW_{th}
Compression chiller	375 €/$kW_{th\text{-}cool}$
CST (concentrated solar thermal) parabolic	3677 €/kW_{el} (without storage) 7254 €/kW_{el} (with storage)
TES	35 €/kWh
Hydrogen storage tank	403 €/kg_{H2}
Hydrogen storage cavern	38 €/kg_{H2}

6.2 Analysis of the results for CAPEX correlations

To better understand the procedure used to derive the previously introduced CAPEX correlations, it is useful to briefly present the output generated by the script's built-in analytical tools and explain how these results should be interpreted.

As an illustrative example, internal combustion engines operating in cogeneration mode with nominal sizes below 500 kW_{el} are considered. Using the input data reported in the script presented earlier, the regression procedures (log–log linear regression and non-linear curve fitting) provide a set of estimated parameters, an indicator (R^2), and the corresponding graphical representations.

The value of R^2 (equal to 0.946) is very close to the target threshold of 0.95 for the log–log linear regression, evaluated in logarithmic space. This indicates that the power-law relationship assumed for the CAPEX scaling is highly consistent with the input data when analyzed in log–log form.

In contrast, R2 associated with the non-linear curve fitting procedure is significantly lower (log-space). This difference highlights how the quality of the fit can vary depending on the regression approach and the space in which the goodness-of-fit is evaluated: while the non-linear method may offer advantages under certain data conditions (e.g., noisy datasets or limited size ranges), in this specific case the log–log linear regression appears to be much more accurate.

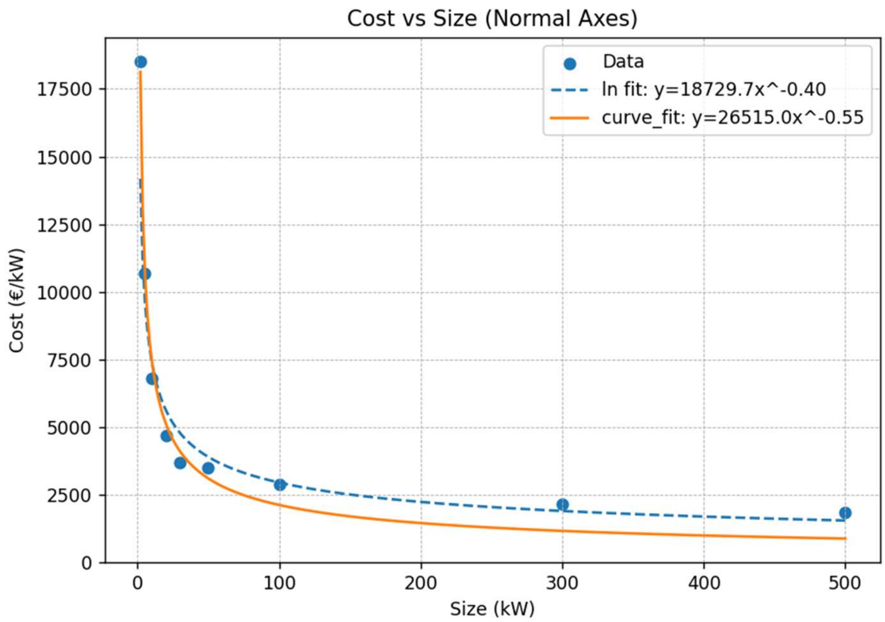

Figure 2: Analysis in linear space (correlation for ICE CHP with size below 500 kW_{el}).

In Figure 2, it is observable that the log–log linear regression provides the most accurate CAPEX correlation for internal combustion engines operating in cogeneration mode with nominal sizes below 500 kW_{el}. Both the graphical comparison and the goodness-of-fit indicators support the selection of this method over the non-linear curve fitting approach for this specific size range.

In conclusion, the selected correlation for ICE CHP units with size lower than 500 kW_{el} is:

$$y = 18729.721 \cdot x^{-0.401}$$

where:

- y is the specific CAPEX, expressed in €/kW_{el},
- x is the nominal electrical size of the unit, expressed in kW_{el}.

As previously discussed, this correlation allows the estimation of the specific investment cost for any unit size within the considered range (below 500 kWel). This provides a practical and reliable tool for cost approximation, avoiding the need to research manufacturer or academic data, which is often scarce and fragmented.

It is important to note that ICE CHP technology required two separate CAPEX correlations, since a single correlation valid for the entire range of 2–10,000 kWel resulted in an unacceptable loss of accuracy. This reduction in precision was clearly evidenced by the plots and by the decrease in R^2.

For the other energy technologies analyzed, however, a single CAPEX correlation was sufficient to maintain a very good level of accuracy (generally $R^2 \geq 0.95$) with respect to the reference data points.

For clarity and completeness, the plots illustrating the linear-space analysis for all energy technologies for which a CAPEX correlation has been derived are provided in Appendix B.

6.3 Analysis of the results for the linearization of performance maps

To assess the accuracy of the linearized performance maps derived using the methodology described above, Table 4 reports the corresponding average and maximum errors. These indicators provide a quantitative measure of the deviation between the original model data and the values reconstructed through the linearized formulation, allowing a clear evaluation of the reliability of the proposed approach across the considered size ranges.

Table 4: Error (percentage) introduced by the linearization of performance maps.

Energy Technology	Size range	Average error	Maximum error
ICE CHP	2 - 100 kW_{el}	3.8% (EE) 1.4% (TH)	10% (EE) 7% (TH)
	100 - 300 kW_{el}	1.6% (EE) 2.4% (TH)	8% (EE) 17% (TH)
	300 - 10000 kW_{el}	1.7% (EE) 1.8% (TH)	8% (EE) 9% (TH)
SOFC CHP	1.5 - 50 kW_{el}	0.4% (EE) 0.7% (TH)	2% (EE) 2% (TH)
	50 - 1000 kW_{el}	3.5% (EE) 1.4% (TH)	11% (EE) 2% (TH)
PEM FC CHP	5 - 120 kW_{el}	0.4% (EE) 0.4% (TH)	5% (EE) 4% (TH)
	120 - 500 kW_{el}	1.6% (EE) 2.0% (TH)	8% (EE) 12% (TH)
NG boiler condensing	10 - 100 kW_{th}	0.5%	3%
	100 - 500 kW_{th}	0.3%	3%
NG boiler non-condensing	500 - 30000 kW_{th}	0.7%	8%
Heat pump (air - water)	5 - 50 kW_{th}	3.7%	8%
	50 - 100 kW_{th}	2.2%	16%
	100 - 300 kW_{th}	3.0%	15%
	300 - 20000 kW_{th}	0.6%	8%

Heat pump (water-water) (large)	1000 - 50000 kW_{th}	2.2%	8%
Geo Water-Water Heat Pump	5 - 100 kW_{th}	1.4%	8%
	100 - 500 kW_{th}	1.7%	8%
	500 - 1000 kW_{th}	2.2%	8%
Alkaline electrolyzer (large)	1-20 MW_{el} (input)	5.9%	8%
PEM electrolyzer (large)	1-20 MW_{el} (input)	6.5%	12%
Wood Chip Boiler	20 - 120 kW_{th}	0.2%	1%
	120 - 1500 kW_{th}	0.6%	8%
Pellet Boiler	10 - 150 kW_{th}	1.0%	14%
Biomass ORC	1-5 MW_{el}	4.5% (EE) 0.7% (TH)	14% (EE) 1% (TH)
	5-10 MW_{el}	3.0% (EE) 0.5% (TH)	10% (EE) 1% (TH)
Absorption chiller (water)	1000 - 10000 kW_{th}	1.3%	6%
Absorption chiller (steam)	1000 - 20000 kW_{th}	0.4%	11%
Compression chiller (large)	50 - 10000 kW_{th}	3.6% (water) 3.1% (air)	6% (water) 9% (air)

The reported errors are calculated by comparing the reference output values (at nominal and minimum part-load operation) with the corresponding values obtained using the linearized model based on the coefficients k_1, k_2, k_3. In other words, once the coefficient set is determined through the least-squares method, the outputs are recalculated using the proposed linear formulation and then compared to the original model data. The relative deviation between these values represents the modeling error.

As highlighted by the results, the average errors are generally very low, confirming that the linearized approach maintains a high degree of accuracy across the size range considered. Although it is true that, for some energy technologies, the maximum error exceeds 10%, this occurs only at one boundary of the considered size range, typically at the lower bound. This behavior is consistent with the limitations of the least-squares fitting procedure, which may be less accurate at the extremes of the dataset. However, the low average errors confirm that the overall accuracy of the method remains high across the majority of the size interval, ensuring that the adopted correlations provide a reliable representation of the technologies within their intended application range. In conclusion, the overall performance of the method demonstrates that the adopted formulation is robust and sufficiently precise for representing part-load behavior.

In most cases, adopting a single set of coefficients k_1, k_2, k_3 over the entire range of sizes would not guarantee a sufficiently accurate representation of part-load and/or nominal performance, particularly when imposing a target average error threshold equal or below 5%. The only possible solution to maintain this desired level of accuracy is to divide the overall size domain into smaller sub-ranges. For this reason, many energy technologies are characterized by more than one set of coefficients, each corresponding to a specific size interval. This subdivision allows the linearized formulation to maintain high fidelity with the reference data, while keeping the number of sub-ranges introduced as low as possible.

For completeness and transparency, all coefficient sets, together with their corresponding error analyses, are reported in Appendix A.

6.3.1 Graphic representations of the errors introduced by the linearization of performance maps

For a clearer representation of the errors introduced by the linearization of the performance maps, the two plots shown in Figure 3 are provided. These plots refer to internal combustion engines operating in cogeneration mode with nominal sizes below 50 kWel. In the figures, the real data points, corresponding to those grouped in the fixed-size database, are represented by colored markers, while the performance profiles reconstructed using the coefficient set (k1, k2, k3) are depicted by dotted lines of the same color. This graphical comparison allows a direct visual assessment of the deviation between the original model data and the linearized approximation.

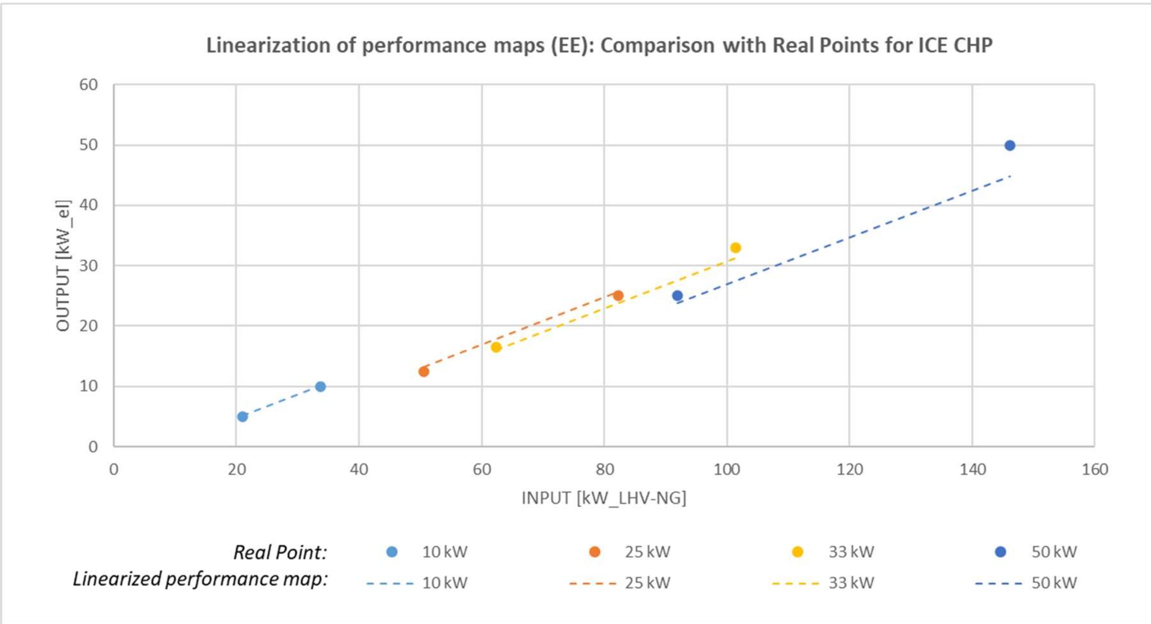

(a) Linearization of performance maps: comparison with real data points (EE) for small ICEs CHP.

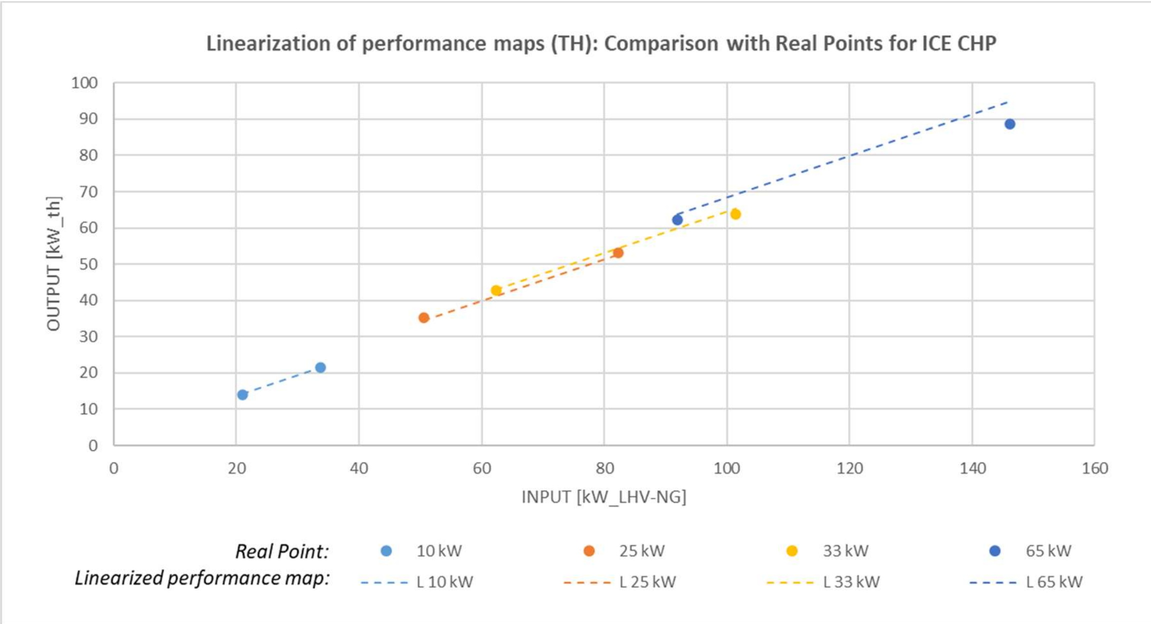

(b Linearization of performance maps: comparison with real data points (TH) for small ICEs CHP.

Figure 3: Linearization of performance maps: comparison with real data points for ICEs CHP.

As shown in Figure 3, the overall accuracy of the method is high. The maximum error remains below 10%, occurring at the nominal operating point of the 50 kWel internal combustion engine model. This confirms that the linearized formulation provides a reliable representation of performance within the considered size range.

Another example is presented in Figure 4, this time referring to natural gas condensing boilers with nominal sizes below 110 kWth.

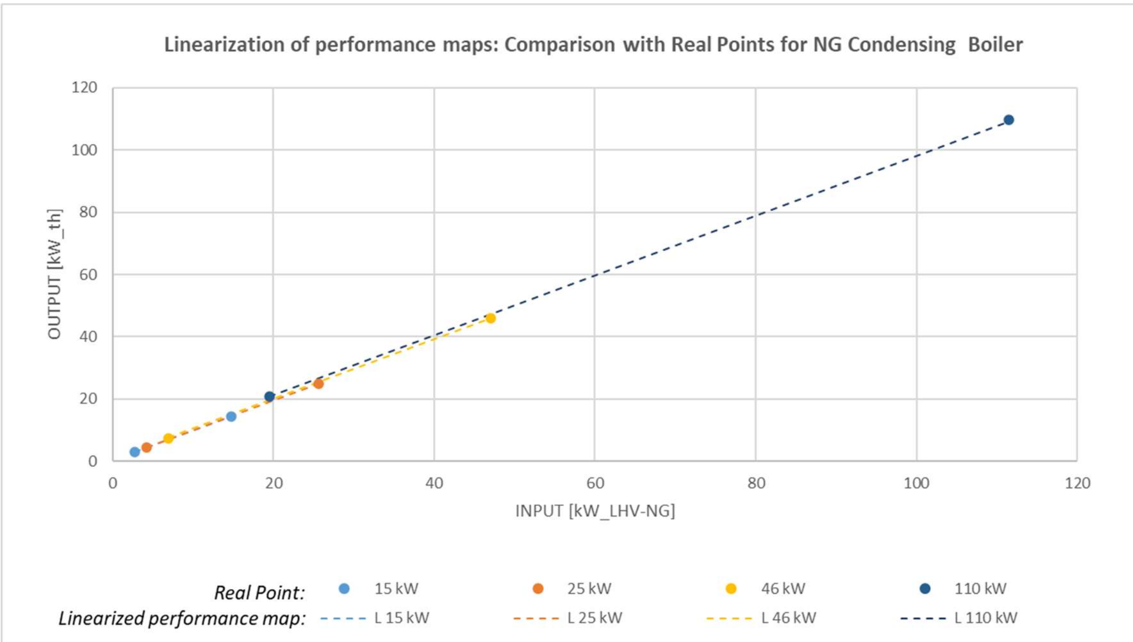

Figure 4: Linearization of performance maps: comparison with real data points for (small) natural gas condensing boilers.

In this case, the average error is lower than 1%, indicating a very high level of accuracy in the linearized performance representation: this is clearly visible in the plot, where the dotted lines obtained through the coefficient set (k_1, k_2, k_3) closely overlap the real performance data.

7. Application of the Technology Database to a case study

The technology database developed in the previous sections is now applied to a representative case study, modeled after a hospital located in Northern Italy. The hourly energy demands considered for this case study are summarized in Table 5.

Table 5: Energy demands.

	Peak [MW]	Total energy demand [MWh/y]
EE	5.00	25072
Heat	10.37	36014
Cooling	9.94	9360

The optimization process must ensure that the final system configuration satisfies all the specified energy demands: electricity, heat, and cooling, continuously and reliably for every hour of the year.

7.1 Input and options applied to My-AESOPT

For each hour of the year, the electricity, heating, and cooling demands are defined and provided as input to My-AESOPT. In addition to the hourly load profiles, the following time-dependent parameters are also specified: ambient temperature, electricity purchase and selling prices with the grid, and the ratio between the actual PV power output and the installed peak power. All these variables are supplied on an hourly basis for the entire year, ensuring a detailed and realistic representation of operating conditions.

Based on these inputs, My-AESOPT assigns a set of typical days to represent the annual profiles. The number of typical days is defined by the user in the input settings. Increasing the number of typical days improves the accuracy of the result but also increases the computational effort required for the optimization process. For the present case study, the number of typical days has been set to six, providing a suitable balance between solution accuracy and computational efficiency.

Additionally, the extreme days option has been activated for heating and cooling demands. This feature allows the software to model peak demand conditions by introducing representative extreme days, ensuring that the system is correctly sized to handle maximum thermal and cooling loads. The extreme days option has not been applied to electricity demand as, in periods of peak electrical demand, purchasing electricity from the grid remains a feasible solution.

Finally, the investment horizon considered for the optimization is set to 25 years, allowing the model to evaluate long-term economic performance and technology selection over a realistic project lifetime.

7.2 Selected energy technologies

Considering the geographical and context of the case study (Northern Italy), the following dispatchable energy technologies have been selected as candidate units for the final system configuration:

- ICE CHP (internal combustion engines for cogeneration),
- SOFC CHP (solid oxide fuel cells for cogeneration),
- PEMFC CHP (proton-exchange membrane fuel cells for cogeneration),
- Water–water heat pumps (for both heating and cooling),
- Compression chillers,
- Absorption chillers,
- Natural gas condensing boilers,
- Natural gas non-condensing boilers,
- Alkaline electrolyzers,
- PEM electrolyzers (proton-exchange membrane electrolyzers).

Among non-dispatchable technologies, photovoltaic (PV) panels are included as a possible generation option, with their hourly production profile determined by the solar availability ratio provided in the input data.

Regarding energy storage technologies, the following solutions have been considered as candidates for the optimal configuration:

- Battery Energy Storage Systems (BESS), with two alternatives: C-rate = 0.5 and C-rate = 0.25,
- Thermal Energy Storage (TES),
- Hydrogen storage tanks.

The final decision on whether to install any of these technologies, together with their optimal sizes and operating strategies, is determined by the optimization process performed by My-AESOPT.

Furthermore, a carbon tax has been applied to all technologies that produce direct CO_2 emissions during operation (ICE CHP, SOFC CHP, and both condensing and non-condensing natural gas boilers). This is not true for the reference case, in which the carbon tax is set to zero in order to provide a baseline comparison.

Electricity imported from the grid is also associated with an emission factor equal to 0.315 ton_{CO2}/MWh [45], corresponding to the current emission factor of the Italian grid. This parameter allows the model to consistently account for indirect emissions when evaluating environmental and economic trade-offs.

7.3 Reference configuration

The reference configuration, as previously discussed, does not include any carbon tax.

As shown in Table 6, the optimal configuration identified by My-AESOPT under this assumption includes the following technologies: natural gas non-condensing boilers, natural gas condensing boilers, ICE CHP units, compression chillers, PV panels, and thermal energy storage (TES).

Table 6: Reference configuration.

Energy Technology	Size unit 1 [MW]	Size unit 2 [MW]	Size unit 3 [MW]	Size unit 4 [MW]	Size unit 5 [MW]
NG non-condensing boilers	3.95	\	\	\	\
NG condensing boilers	0.50	0.50	0.50	0.50	0.50
ICEs CHP	2.45 (EE) 2.67 (Heat)	\	\	\	\
Compression chillers	7.47	2.47	\	\	\
PV panels	12.36	\	\	\	\
TESs	12.07 MWh	\	\	\	\

In the absence of a carbon tax, fossil-fuel-based technologies for electricity and heat production become more economically attractive. Although they are characterized by higher operational costs due to fuel consumption, their relatively low capital investment costs make them more competitive than alternative solutions such as heat pumps for thermal production. As a result, the optimization process favors these technologies in the reference scenario.

The maximum installable PV capacity for the hospital considered in the case study is 12.36 MWp. Owing to the relatively low specific CAPEX of PV systems, the optimizer selects the maximum available capacity even when no carbon tax is applied.

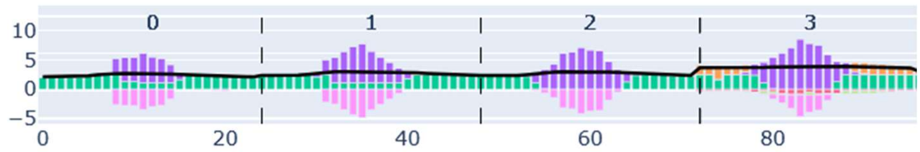

(a) Electrical Power Balance (typical days 0, 1, 2, 3).

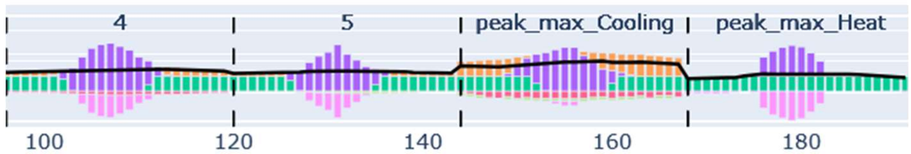

(b) Electrical Power Balance (typical days 4, 5, peak cooling day, peak heat day).

(c) Legend.

Figure 5: Electrical Power Balance.

In Figures 5, the electrical power balance can be analyzed in detail. During daytime hours, when PV panels are active, they fully cover the hospital's electrical demand as well as the electricity required by the compression chillers when they are operating. Any surplus electricity produced, up to a maximum of approximately 4.8 MW_{el}, is exported to the grid.

When PV production is unavailable, the electrical demand is primarily covered by the internal combustion engine (ICE CHP) and, when necessary, by electricity purchased from the grid. The dissipation associated with the ICE is negligible and therefore only marginally visible in the corresponding plot.

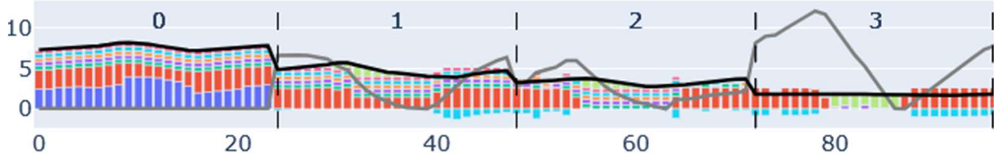

(a) Heat Power Balance (typical days 0, 1, 2, 3).

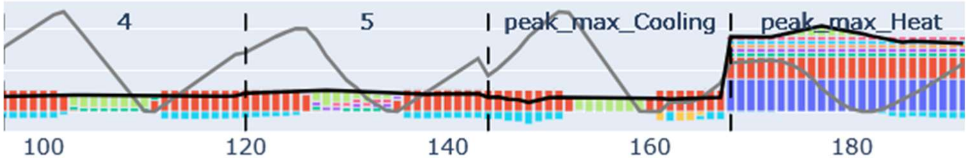

(b) Heat Power Balance (typical days 4, 5, peak cooling day, peak heat day).

(c) Legend.

Figure 6: Heat Power Balance.

As shown in Figure 6, the heat demand is entirely satisfied by the combination of natural gas boilers (both condensing and non-condensing), the ICE CHP unit, and the thermal energy storage (TES) system. The TES typically discharges during the middle of the day, when thermal demand is lower and previously stored heat can be effectively utilized. Also in this case, the thermal dissipation from the ICE and boilers is minimal and therefore barely noticeable in the graphical representation.

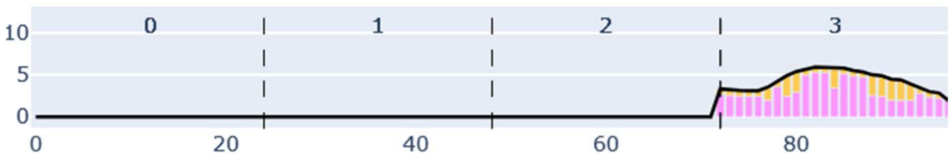

(a) Cooling Power Balance (typical days 0, 1, 2, 3).

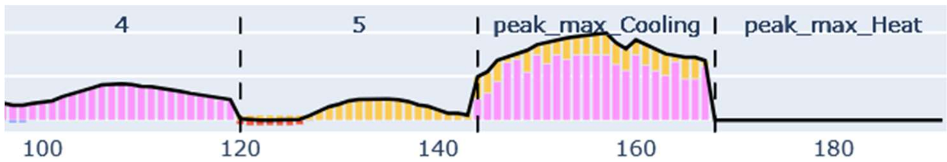

(b) Cooling Power Balance (typical days 4, 5, peak cooling day, peak heat day).

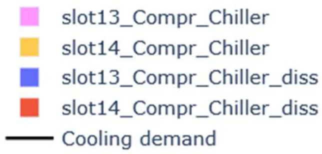

(c) Legend.

Figure 7: Cooling Power Balance.

Finally, as illustrated in Figure 7, the cooling demand is fully covered by the two compression chillers. The associated dissipation is very limited and consequently scarcely visible in the plot, confirming the overall effective matching between cooling production and demand within the optimized configuration.

7.4 Optimal configuration

For this optimization scenario, a carbon tax equal to 92.2 €/ton$_{CO_2}$ [46] has been applied to all energy technologies that produce direct CO_2 emissions during operation (ICE CHP, SOFC CHP, and both condensing and non-condensing natural gas boilers). This additional cost penalizes fossil-fuel-based technologies from an economic point of view. As a consequence, energy units that were previously considered too expensive by My-AESOPT become economically viable in the new optimal configuration (such as heat pumps), as presented in Table 7.

Table 7: Optimal configuration.

Energy Technology	Size unit 1 [MW]	Size unit 2 [MW]
NG non-condensing boilers	1.43	\
Water-Water Heat Pump (Heating)	6.18	\

ICEs CHP	1.36 (EE) 1.52 (Heat)	\
Compression chillers	7.47	2.47
PV panels	12.36	\
TESs	10.70 MWh	\
BESS **(C-rate = 0.5)**	7.69 MWh	\

The introduction of the carbon tax leads to a significantly different system layout. All natural gas condensing boilers are excluded from the optimal configuration, while the installed capacity of non-condensing boilers is reduced by more than half compared to the reference case. The portion of heat demand no longer supplied by these boilers is instead covered by a water–water heat pump, which becomes economically competitive once the carbon cost is added. This shift is clearly illustrated in Figures 8, where the thermal power balance is presented.

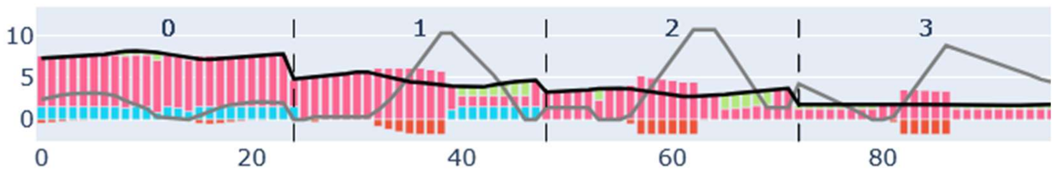

(a) Heat Power Balance (typical days 0, 1, 2, 3).

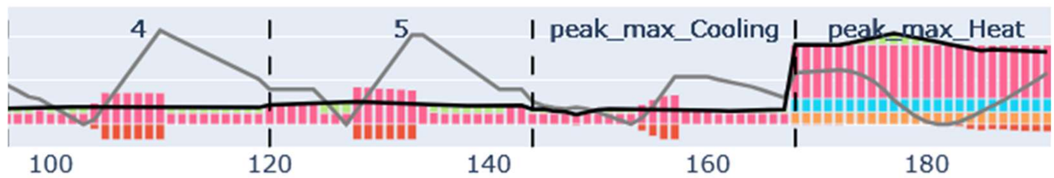

(b) Heat Power Balance (typical days 4, 5, peak cooling day, peak heat day).

(c) Legend.

Figure 8: Heat Power Balance.

The carbon tax also shifts the system toward a greater reliance on electricity as the main energy vector, reducing dependence on natural gas. As a result, the installed capacity of ICE CHP units decreases, and a Battery Energy Storage System (BESS) becomes part of the optimal configuration. The BESS enables temporal shifting of electrical energy, improving the utilization of locally generated electricity and enhancing operational flexibility.

The combined introduction of BESS and the heat pump would reduce the amount of electricity exported to the grid, but the smaller ICE CHP capacity ultimately increases reliance on grid electricity, particularly during the early and late hours of the day. This outcome is consistent with the applied carbon pricing: even when accounting for the grid emission factor, purchasing electricity from the grid becomes more economically favorable than producing it locally using natural gas-based technologies under a carbon tax regime. These trends are confirmed by Figures 9, which show the electrical power balance.

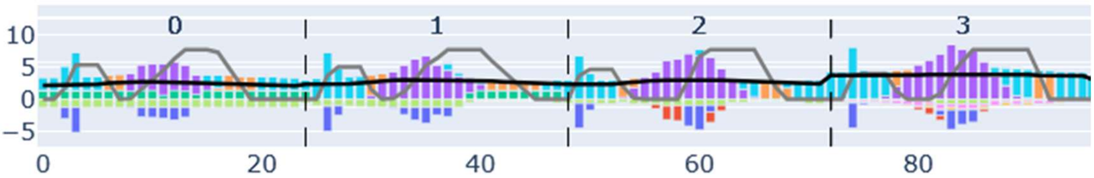

(a) Electrical Power Balance (typical days 0, 1, 2, 3).

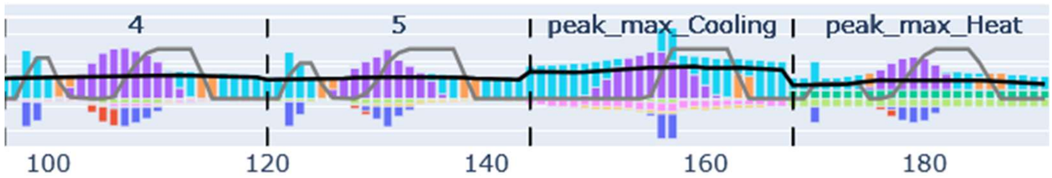

(b) Electrical Power Balance (typical days 4, 5, peak cooling day, peak heat day).

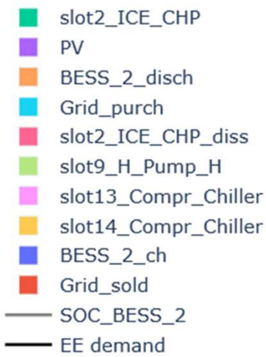

(c) Legend.

Figure 9: Electrical Power Balance.

Photovoltaic panels, compression chillers, and thermal energy storage (TES) remain largely unchanged between the reference and carbon-tax scenarios. The slight reduction in TES capacity can be attributed to the introduction of the BESS and the water–water heat pump. The increased electrification of heat production and the improved temporal management of electricity reduce the need for thermal buffering, as part of the system flexibility is now provided electrically rather than thermally.

The cooling demand profile remains essentially identical to that of the reference configuration, as the same two compression chillers, unchanged in size, continue to satisfy the entire cooling load.

7.5 NPC and emissions comparison

It is particularly meaningful to compare the two configurations in terms of CO_2 emissions and Net Present Cost (NPC): the introduction of the carbon tax results in a 47.6% reduction in total CO_2 emissions, while the NPC increases by only 6.5% compared to the reference configuration, as it can be seen in Table 8.

Table 8: CO_2 Emissions and NPC comparison.

Configuration	CO_2 Emissions [kton/y]	NPC [M€]
Reference	12.01	74.387
Optimal	6.29	79.526

This outcome highlights a key result of the optimization process: a substantial reduction in environmental impact can be achieved with a relatively limited increase in overall system cost. The modest rise in NPC reflects the higher investment in low-emission technologies (such as heat pumps and electrical storage) and the reduced reliance on fossil-fuel-based generation.

These results demonstrate the capability of My-AESOPT to identify balanced solutions that significantly reduce emissions without imposing disproportionate economic penalties, supporting the feasibility of decarbonization strategies in complex energy systems.

7.6 Notes on the results

Although the selected water–water heat pumps are technically capable of producing both heating and cooling, this dual functionality is not currently configurable within My-AESOPT. At present, if both heating and cooling outputs are required from heat pumps, the model must treat them as two separate units: one dedicated to heating and the other to cooling.

Because of this modeling limitation, and given that compression chillers exhibit lower investment costs than heat pumps when configured solely for cooling, My-AESOPT correctly selects compression chillers to meet the cooling demand in the optimized configuration. From the model's perspective, this is the most economically convenient solution under the current assumptions.

However, in real-world applications, a reversible water–water heat pump capable of delivering both heating and cooling within a single integrated system could potentially represent a more cost-effective solution than standalone compression chillers. This would be particularly relevant in the present case study, where a heat pump is already installed for heating purposes in the carbon-tax scenario. Allowing a single unit to operate in both modes could improve overall system integration, increase utilization rates, and potentially reduce total investment costs.

8. Conclusions

This work aimed to develop and implement a comprehensive technology database to support the optimization process performed by My-AESOPT for Aggregated Energy Systems (AES). To ensure robustness and reliability, only data from reputable manufacturers and well-established academic sources were considered in the construction of the database.

The application of the database to the case study returned promising results, demonstrating that significant reductions in AES CO_2 emissions can be achieved with only a marginal increase in investment costs, thanks to the optimization capabilities of My-AESOPT. The consistency of the results also supports the validity and reliability of the input data adopted for the analysis.

Future research could focus on continuously updating and refining the database, as the energy technology landscape is rapidly evolving. Improvements in performance, cost reductions, and emerging technologies should be periodically incorporated to maintain the accuracy and relevance of the database.

9. Bibliography

[1] P. Mancarella, "MES (multi-energy systems): An overview of concepts and evaluation models," 2014. [Online]. Available: http://dx.doi.org/10.1016/j.energy.2013.10.041.

[2] V. Dipierro, "My-AESOPT: A systematic approach for the optimal investment planning and design of aggregated energy systems," 2025. [Online]. Available: https://www.sciencedirect.com/science/article/pii/S0306261925017362.

[3] H. Hakonen, "An efficient linear programming algorithm for combined heat and power production," 2003.

[4] R. Yokoyama, "A MILP decomposition approach to large scale optimization in structural design of energy supply systems," 2002.

[5] M. Zatti, "Optimal design of urban energy districts under uncertainty," 2019. [Online]. Available: https://www.politesi.polimi.it/handle/10589/148435.

[6] KWW-Halle, "Technology Catalog – Heat Planning, Version 1.1, August 2024, CC-BY, and 2025 edition (october 2025)," [Online]. Available: https://www.kww-halle.de/praxis-kommunale-waermewende/bundesgesetz-zur-waermeplanung.

[7] Totem, "Totem Datasheets," [Online]. Available: https://www.totem.energy/totem_gamma/. [Accessed November 12 2025].

[8] Hydrogen Europe, "Hydrogen Europe - Strategic Research and Innovation Agenda," [Online]. Available: https://hydrogeneurope.eu/wp-content/uploads/2021/11/20201027-SRIA-CHE-final-draft.pdf.

[9] NREL, "Scattergood Modernization Project Alternatives: Summary of Findings," [Online]. Available: https://www.ladwp.com/sites/default/files/2025-03/Scattergood%20Moderniazation%20Alternative%20Study%20Final.pdf.

[10] Convion, "Convion C60," [Online]. Available: https://convion.fi/wp-content/uploads/2023/09/Convion_C60_brochure_2023.pdf.

[11] JRC, "Historical Analysis of FCH 2 JU Stationary Fuel Cell Projects," [Online]. Available: https://publications.jrc.ec.europa.eu/repository/bitstream/JRC125018/stationary_kpi_report_-_18052021_-_public_version_with_identifiers.pdf.

[12] European Hydrogen Observatory, "Cost of hydrogen production - European Hydrogen Observatory," [Online]. Available: https://observatory.clean-hydrogen.europa.eu/hydrogen-landscape/production-trade-and-cost/cost-hydrogen-production.

[13] PowerCell Group, "Zero-Emission Power Generation Solutions," [Online]. Available: https://powercellgroup.com/segments/power-generation/.

[14] Hoval, "Hoval UltraGas Description (15-100) Floor-standing gas condensing boiler," [Online]. Available: https://edergen.be/uploads/downloads/Hoval-UltraGas-15-100-EN.pdf.

[15] CBLE, "CBLE Firetube Boiler," [Online]. Available: https://cleaverbrooks.com/Catalog/boilers/firetube/cble.

[16] R. O'Hegarty, "Air-to-water heat pumps: Review and analysis of the performance gap between in-use and product rated performance," [Online]. Available: https://www.sciencedirect.com/science/article/abs/pii/S1364032121011540.

[17] TRANE, "Ecodesign Datasheet Management," [Online]. Available: https://ecodesign.tranetechnologies.com/ords/r/stsbx/ecodesigndatasheetmgmt/home. [Accessed 11 December 2025].

[18] NREL, "End-Use Savings Shapes Measure Documentation: Central Hydronic Water-to-Water Geothermal Heat Pump," [Online]. Available: https://docs.nrel.gov/docs/fy24osti/89239.pdf.

[19] AURECON, "2020 Costs and Technical Parameter Review," [Online]. Available: https://www.aemo.com.au/-/media/files/electricity/%E2%80%8Cnem/%E2%80%8Cplanning_and_%E2%80%8Cforecasting/%E2%80%8Cinputs-assumptions-methodologies/%E2%80%8C2021/Aurecon-Cost-and-Technical-Parameters-Review-2020.pdf.

[20] A. Christensen, "Assessment of Hydrogen Production Costs from Electrolysis: United States and Europe," [Online]. Available: https://theicct.org/wp-content/uploads/2021/06/final_icct2020_assessment_of-_hydrogen_production_costs-v2.pdf.

[21] Thyssenkrup, "Hydrogen from large-scale electrolysis," [Online]. Available: https://ucpcdn.thyssenkrupp.com/_binary/UCPthyssenkruppBAISUhdeChlorineEngineers/

en/products/water-electrolysis-hydrogen-production/alkaline-water-electrolysis/link-thyssenkrupp_Hydrogen_Water_Electrolysis_and_green_chemicals.pdf.

[22] Accellera, "PEM Electrolyzers HyLYZER Series," [Online]. Available: https://www.accelerazero.com/sites/default/files/2023-03/Electrolyzer%20Technologies%20-%20Brochure%20-%20Accelera%20by%20Cummins%20-%2003%2003%202023_0.pdf?utm_campaign=newpower-accelera-tradeshows&utm_content=&utm_medium=qr-code.

[23] Hargassner, [Online]. Available: https://www.hargassner.com/ca-en/.

[24] KWB, "Wood chip & Pellet heating systems 20 – 150 kW - Technology & Planning 2025," [Online]. Available: https://www.kwb.net/fileadmin/media/EN/Technik_Planung_Anleitungen_PDF/KWB_T_P_EN_04_2025_Modul_E_Wood_chip_and_pellet_Heatings_system_20-150_kW.pdf.

[25] JRC, "Bioenergy in the European Union (2022)," [Online]. Available: https://publications.jrc.ec.europa.eu/repository/bitstream/JRC130730/2022.5470_kjna31283enn.pdf.

[26] K. Qiu, "Biomass-fired Organic Rankine Cycle-based CHP for Community-Scale Applications," [Online]. Available: https://www.energy-proceedings.org/wp-content/uploads/2022/08/MITAB_2022_paper_4117.pdf.

[27] Turboden, "Turboden: ORC Solutions for Cogeneration and District Heating," [Online]. Available: https://iea.blob.core.windows.net/assets/imports/events/122/Alessandro_Foresti_2015_03_23_Kiev.pdf.

[28] US Department of Energy , "Combined Heat and Power Technology Fact Sheet Series," [Online]. Available: https://www.energy.gov/sites/prod/files/2017/06/f35/CHP-Absorption%20Chiller-compliant.pdf.

[29] NREL, "Techno-Economic Analysis for a Potential Geothermal District Heating System in Tuttle, Oklahoma," [Online]. Available: https://docs.nrel.gov/docs/fy24osti/86946.pdf.

[30] Yazaki, "Gruppi refrigeranti alimentati ad acqua calda, Specifiche tecniche," [Online]. Available: https://maya-airconditioning.com/wp-content/uploads/2022/10/1_WFC_MBCE1_Specifiche_tecniche_ver_1_22.pdf.

[31] Thermax, "Direct Fired VAM XP Series," [Online]. Available: https://www.thermaxglobal.com/wp-content/uploads/2024/09/Direct-Fired-Absorption-Chiller-XP-Brochure.pdf.

[32] Siram Veolia, "Siram Veolia Data".

[33] Carrier, "AquaEdge Water-Cooled Centrifugal Chiller 19 MV," [Online]. Available: https://www.carrier.com/commercial/en/us/products/chillers-components/water-cooled-chillers/19mv/.

[34] NREL, "Summer 2024 Solar Industry Update (2024)," [Online]. Available: https://docs.nrel.gov/docs/fy24osti/91209.pdf.

[35] EIA, "Capital Cost and Performance Characteristic Estimates for Utility Scale Electric Power Generating Technologies," [Online]. Available: https://www.eia.gov/analysis/studies/powerplants/capitalcost/pdf/capital_cost_aeo2020.pdf.

[36] NREL, [Online]. Available: https://atb.nrel.gov/electricity/2024b/index.

[37] NREL, "Cost and Performance Assumptions for Modeling Electricity Generation Technologies," [Online]. Available: https://docs.nrel.gov/docs/fy11osti/48595.pdf.

[38] NREL, "Cost of Wind Energy Review: 2024 Edition (2024)," [Online]. Available: https://docs.nrel.gov/docs/fy25osti/91775.pdf.

[39] IRENA, "Renewable power generation costs in 2024 (datafile)," [Online]. Available: https://www.irena.org/Publications/2025/Jun/Renewable-Power-Generation-Costs-in-2024.

[40] PNNL, "2022 Grid Energy Storage Technology Cost and Performance Assessment," [Online]. Available: https://www.pnnl.gov/sites/default/files/media/file/ESGC%20Cost%20Performance%20Report%202022%20PNNL-33283.pdf.

[41] Argonne National Laboratory, "Development of Energy Storage: Cost models," [Online]. Available: https://publications.anl.gov/anlpubs/2021/04/167188.pdf.

[42] NREL, "Re-Designing the CSP Thermal Energy Storage System to Enable HigherTemperature Performance at Reduced Cost: Final Technical Report," [Online]. Available: https://docs.nrel.gov/docs/fy23osti/84409.pdf.

[43] "Hydrogen and Fuel Cell Technologies Office Multi-Year Program Plan (Infrastructure section) (2024)," [Online]. Available: Hydrogen and Fuel Cell Technologies Office Multi-Year Program Plan (Infrastructure section) (2024).

[44] A. Burke, "Hydrogen Storage and Transport: Technologies and Costs (2024)," [Online]. Available: https://escholarship.org/content/qt83p5k54m/qt83p5k54m_noSplash_8bb1326c13cfb9aa3d0d376ec26d3e06.pdf.

[45] Terna, "Confronti internazionali: quadro sintetico di indicatori socioeconomici ed energetici nel mondo per l'anno 2022," 2022. [Online]. Available: https://download.terna.it/terna/Confronti%20internazionali_2022_8ddbb06e029a14b.pdf.

[46] A. Nelli, "Europa: costo delle emissioni CO2 verso i 100 euro," 18 Gennaio 2026. [Online]. Available: https://cronachedi.it/europa-costo-delle-emissioni-co2-verso-i-100-euro/.

Acknowledgements

I would like to express my sincere gratitude to Prof. Emanuele Martelli and Dott. Vincenzo Dipierro for their continuous support and guidance throughout the development of this thesis. Their availability, insightful feedback, and willingness to share their knowledge and expertise have been invaluable to my academic and professional growth. I am especially thankful to them for giving me the opportunity to work on a topic that aligns with my academic interests.

Appendix A

The script mentioned in section 4 can be obtained from the following GitHub repository, along with the Excel sheet with the set of coefficients (k1, k2, k3), and the Technology Database (both Variable-size and fixed-size databases):

https://github.com/MattiaPudduPolimi/Optimization-with-My-AESOPT

Appendix B

The plots illustrating the linear-space analysis, for all energy technologies for which a CAPEX correlation has been derived, are provided in this Appendix.

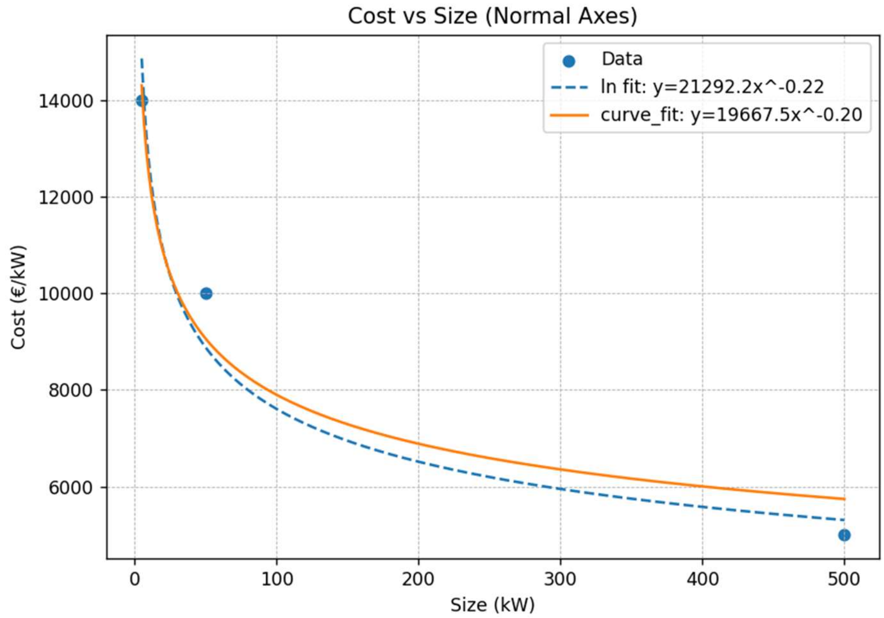

Figure B1: Analysis in linear space (correlation for SOFC CHP).

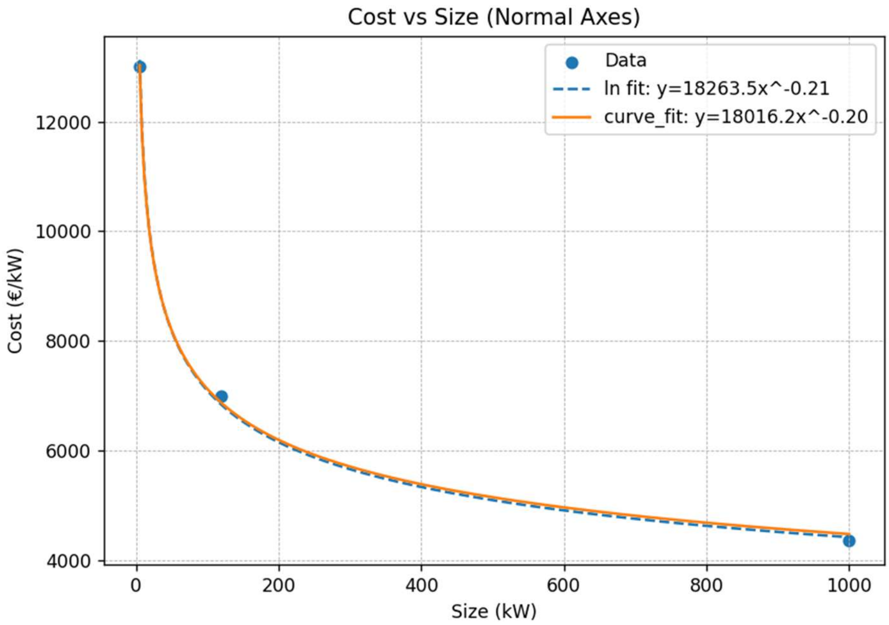

Figure B2: Analysis in linear space (correlation for PEMFC CHP).

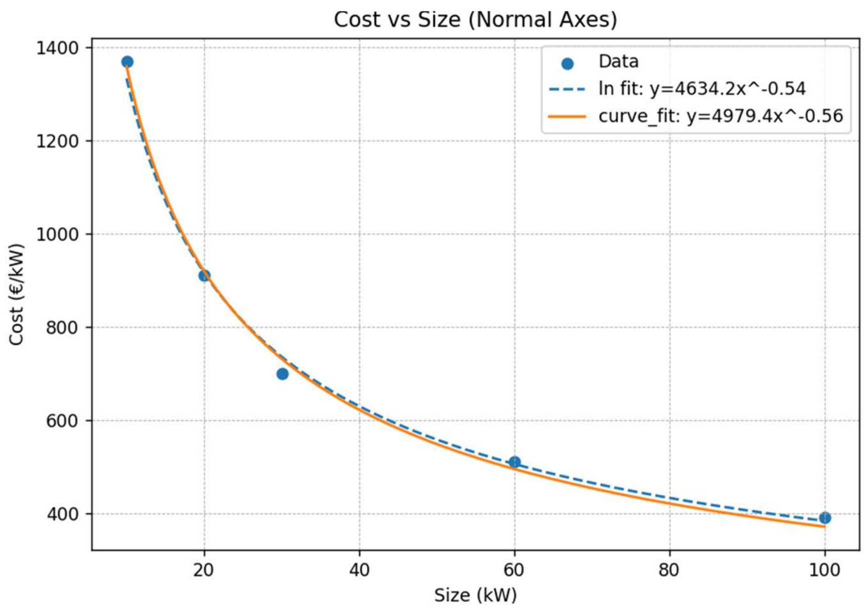

Figure B3: Analysis in linear space (correlation for natural gas condensing boiler).

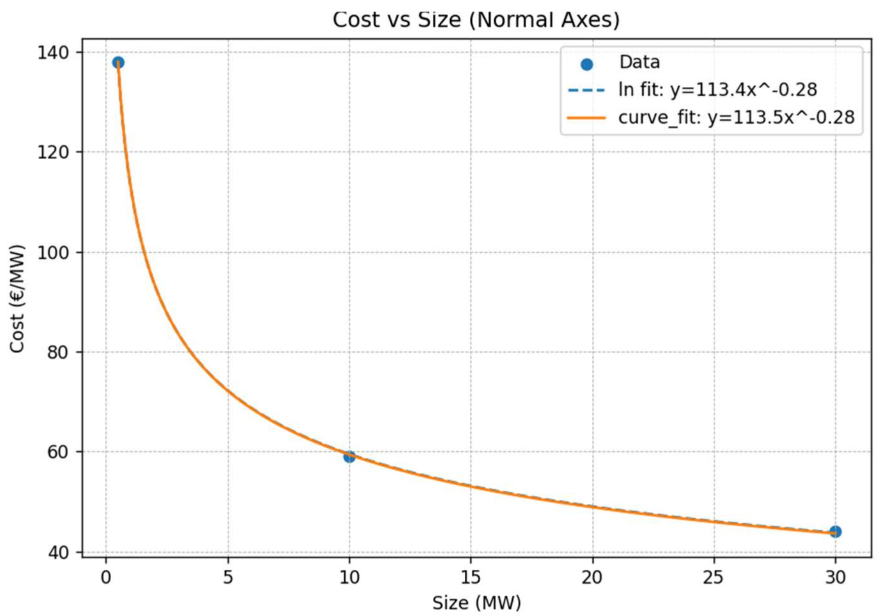

Figure B4: Analysis in linear space (correlation for natural gas non-condensing boiler).

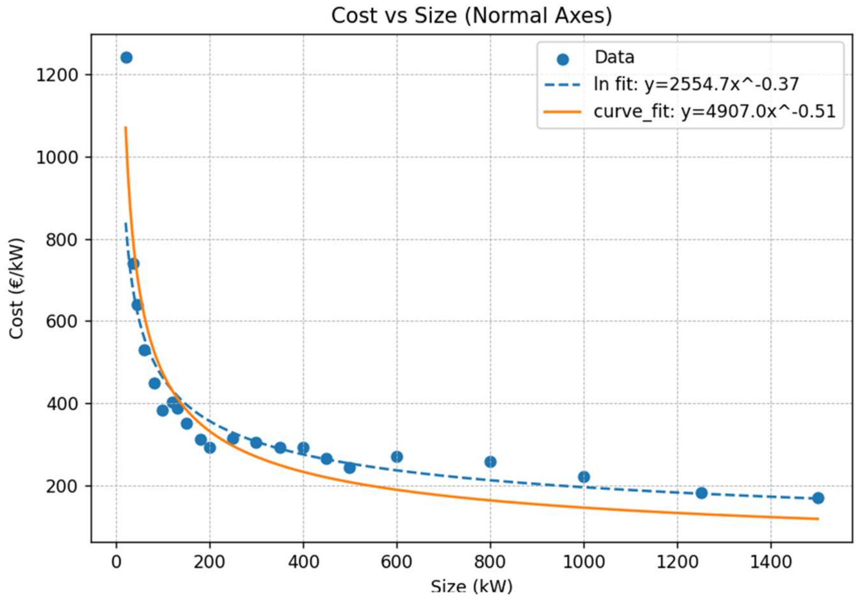

Figure B5: Analysis in linear space (correlation for wood chips boiler).

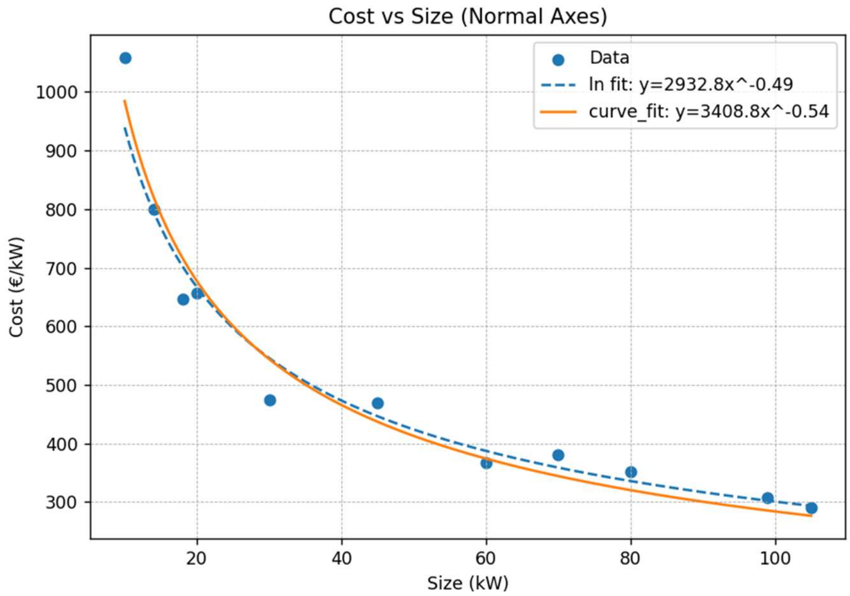

Figure B6: Analysis in linear space (correlation for pellet boiler).

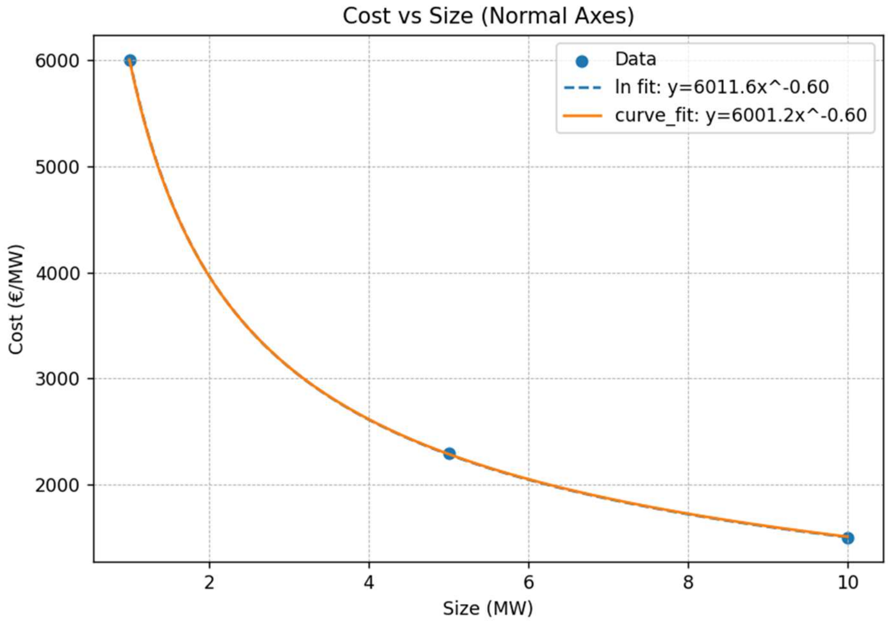

Figure B7: Analysis in linear space (correlation for biomass ORC).

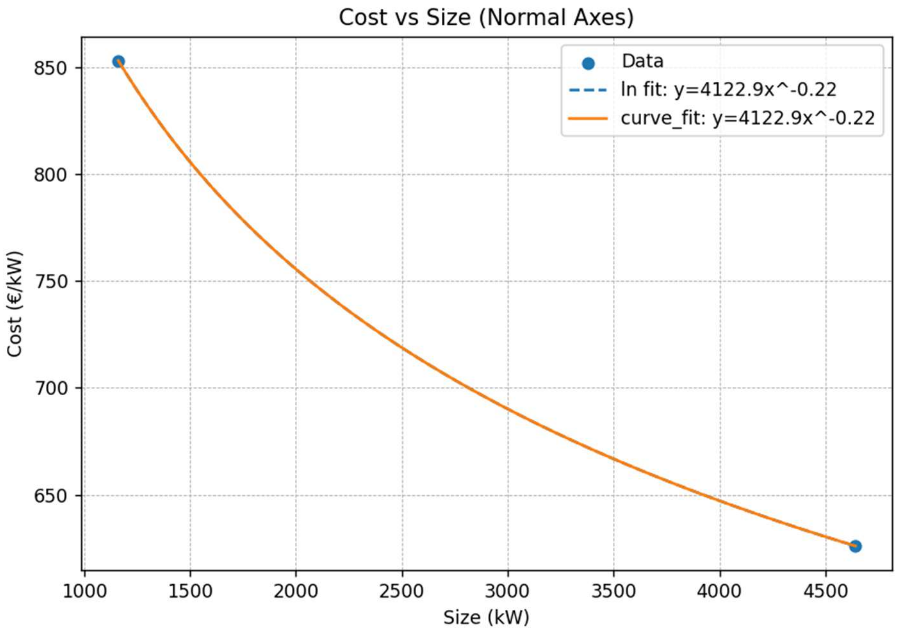

Figure B8: Analysis in linear space (correlation for steam absorption chiller).

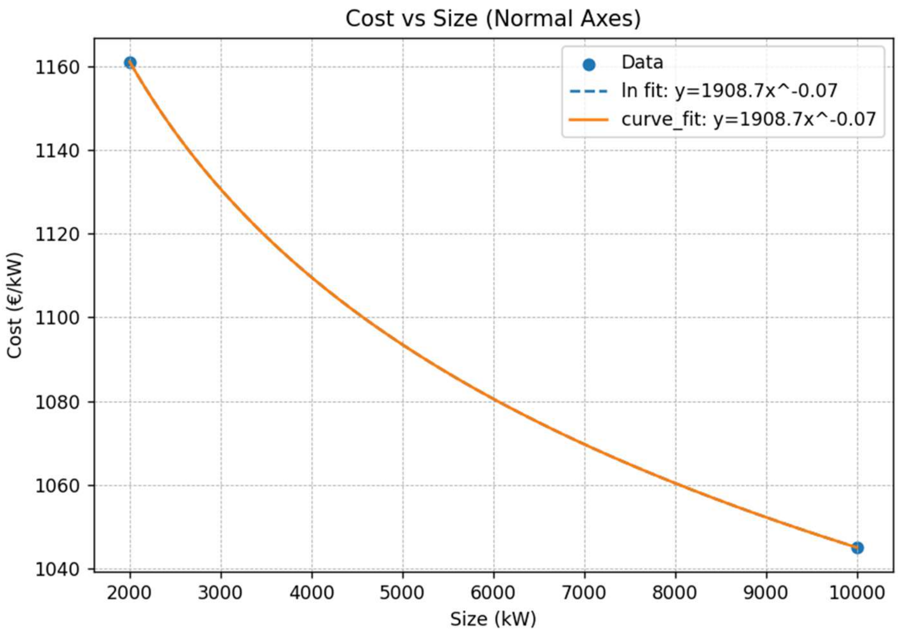

Figure B9: Analysis in linear space (correlation for ICE CHP with size between 500 - 10000 kW_{el}).

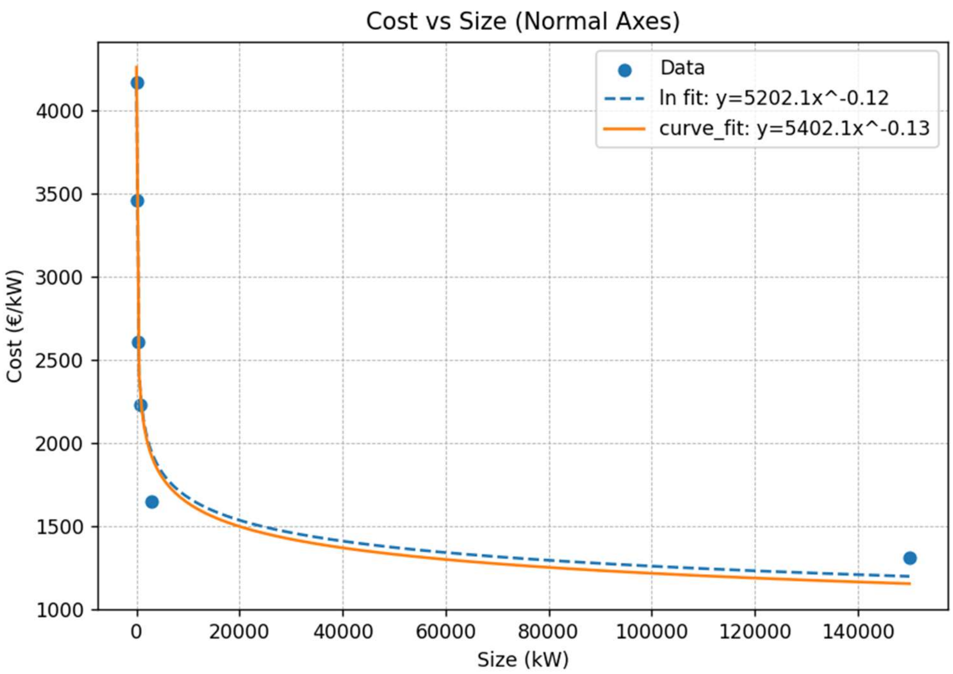

Figure B10: Analysis in linear space (correlation for PV panels).

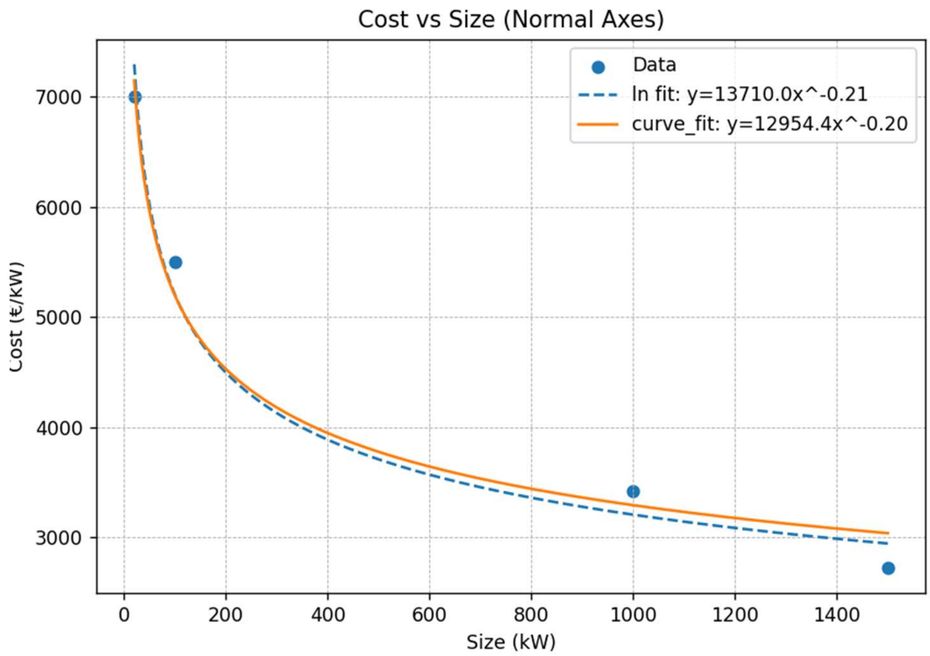

Figure B11: Analysis in linear space (correlation for distributed Wind Turbines).

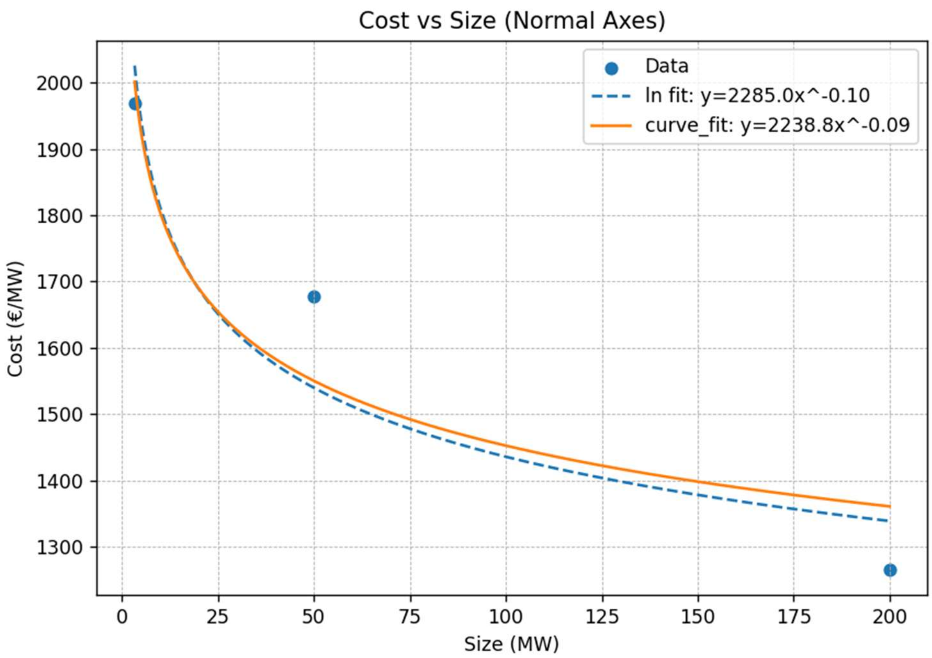

Figure B12: Analysis in linear space (correlation for utility Wind Turbines).

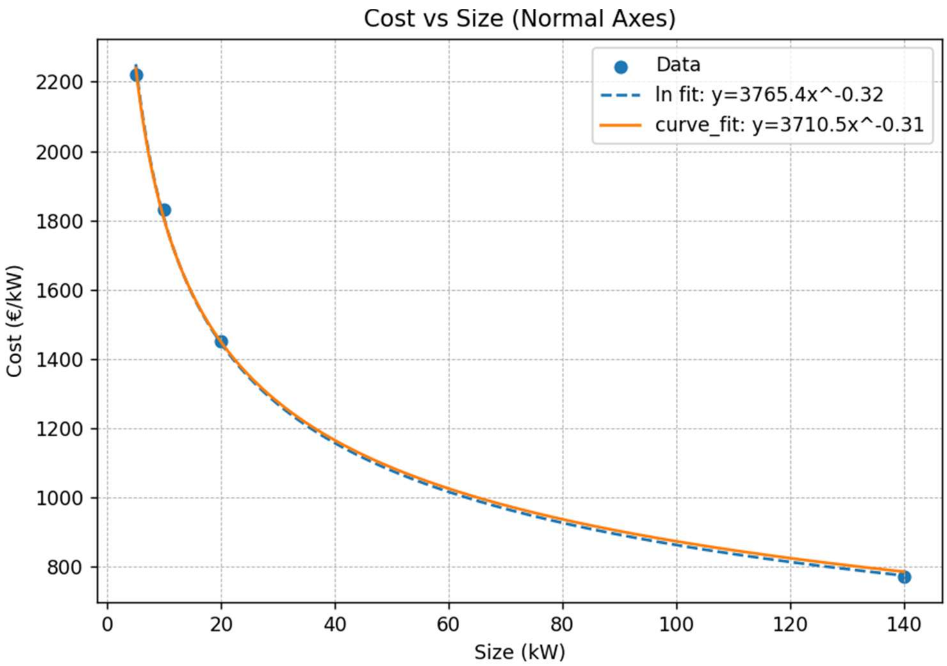

Figure B13: Analysis in linear space (correlation for solar thermal – roof system).

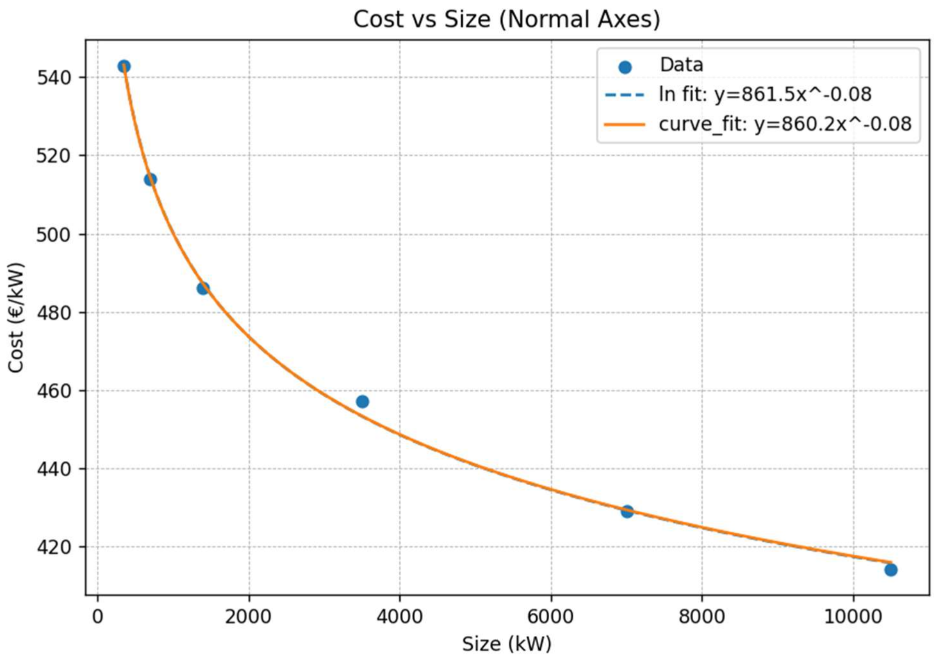

Figure B14: Analysis in linear space (correlation for solar thermal – open-air system).

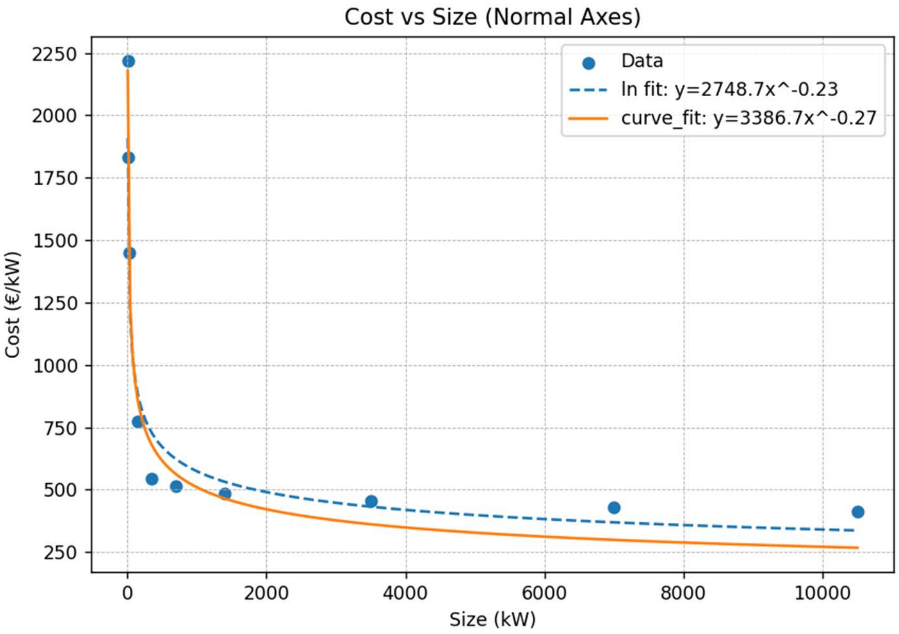

Figure B15: Analysis in linear space (correlation for solar thermal – general).

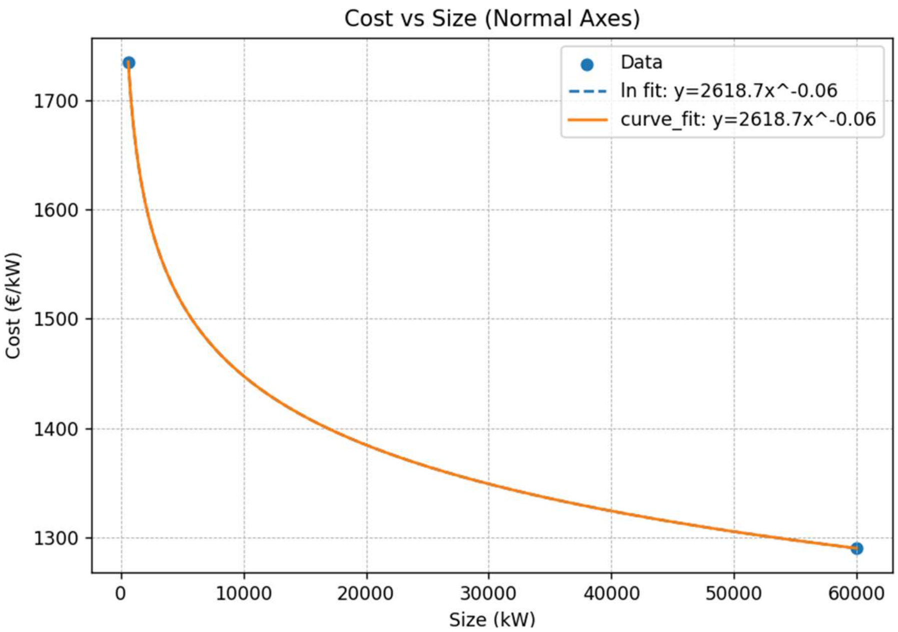

Figure B16: Analysis in linear space (correlation for BESS with C-rate = 0.25).

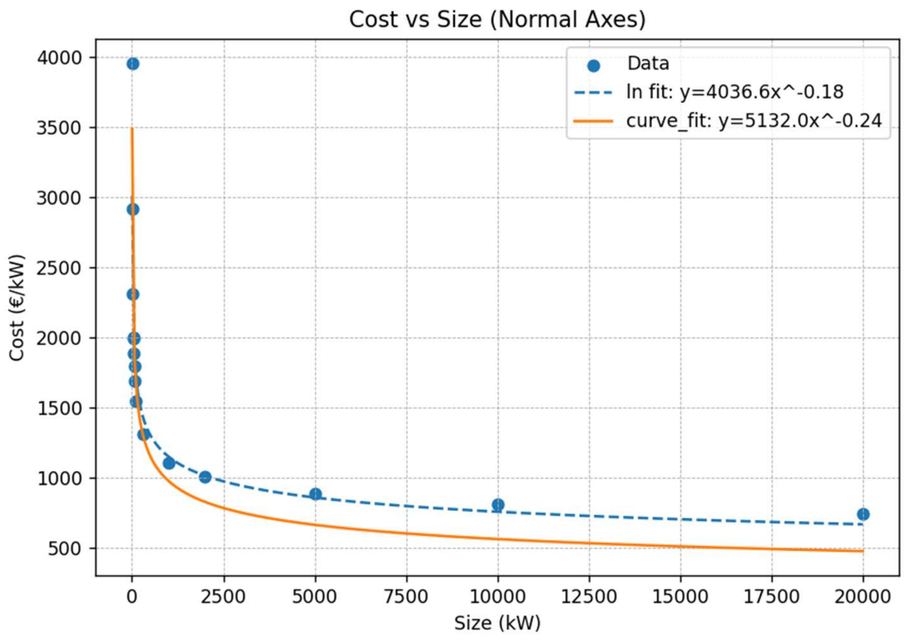

Figure B17: Analysis in linear space (correlation for air-water heat pump, referred to heating).

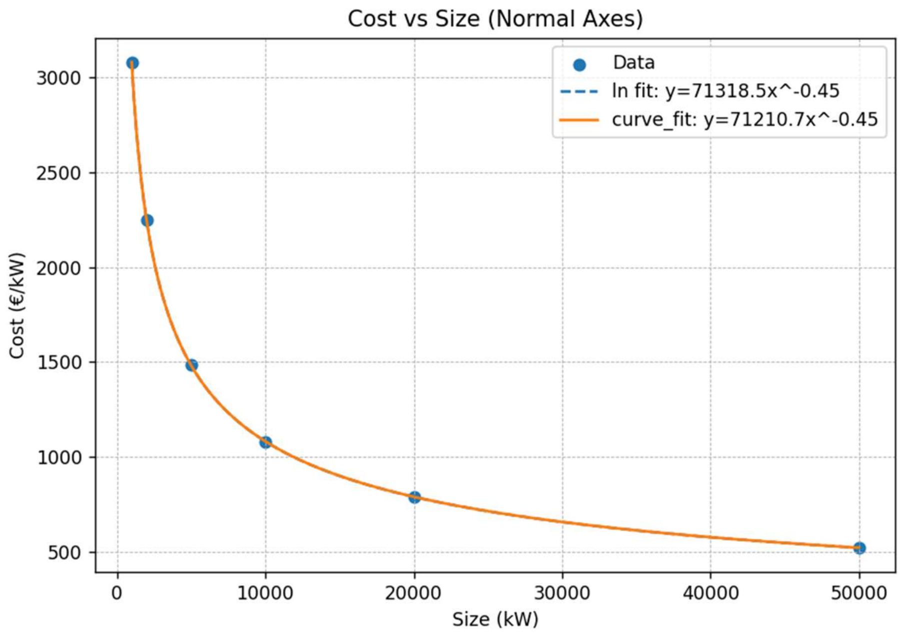

Figure B18: Analysis in linear space (correlation for water-water heat pump, referred to heating).

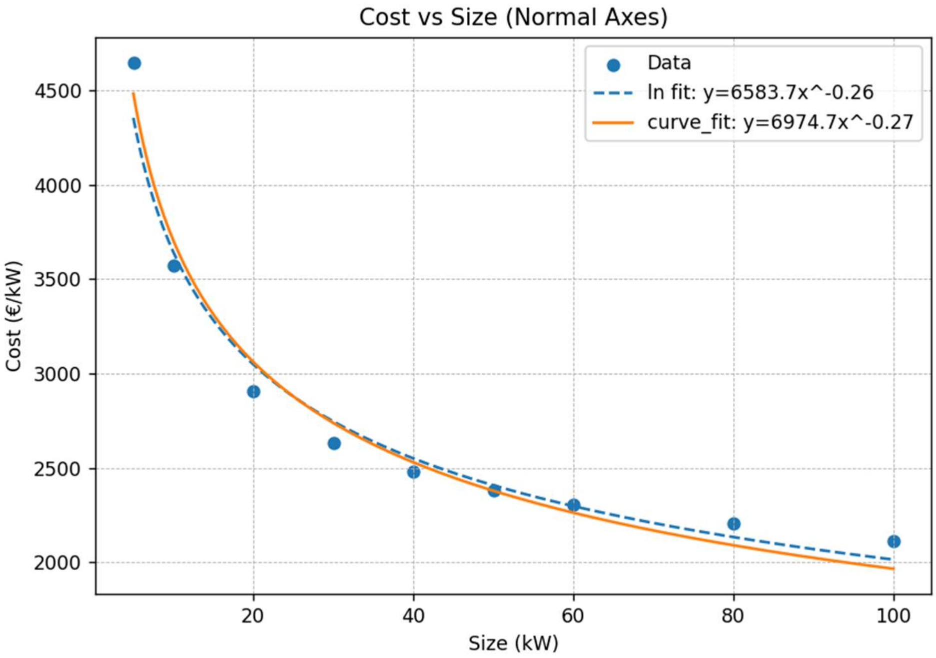

Figure B19: Analysis in linear space (correlation for geothermal heat pump with groundwater well, referred to heating).

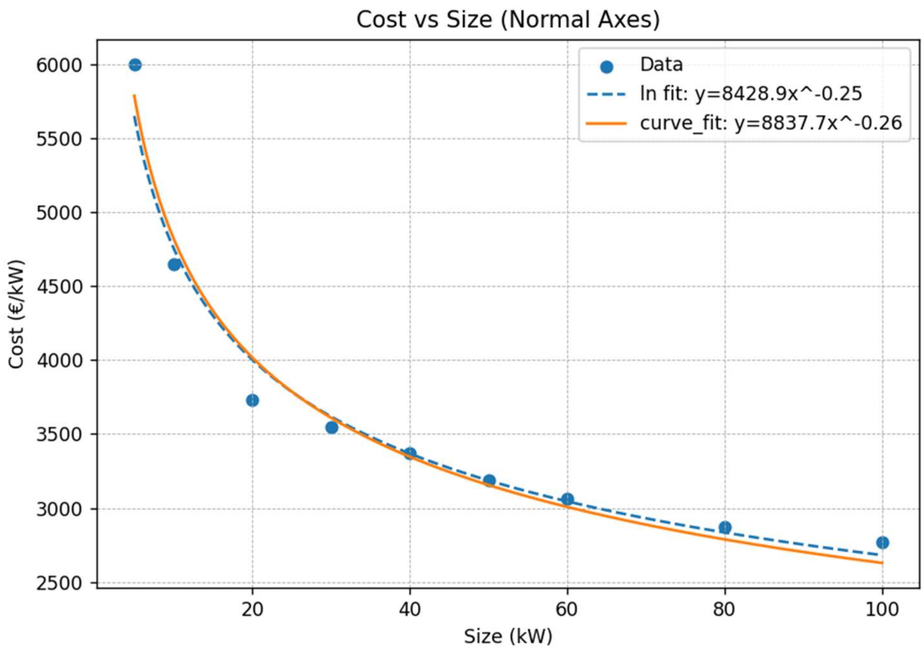

Figure B20: Analysis in linear space (correlation for geothermal heat pump with borehole probes, referred to heating).

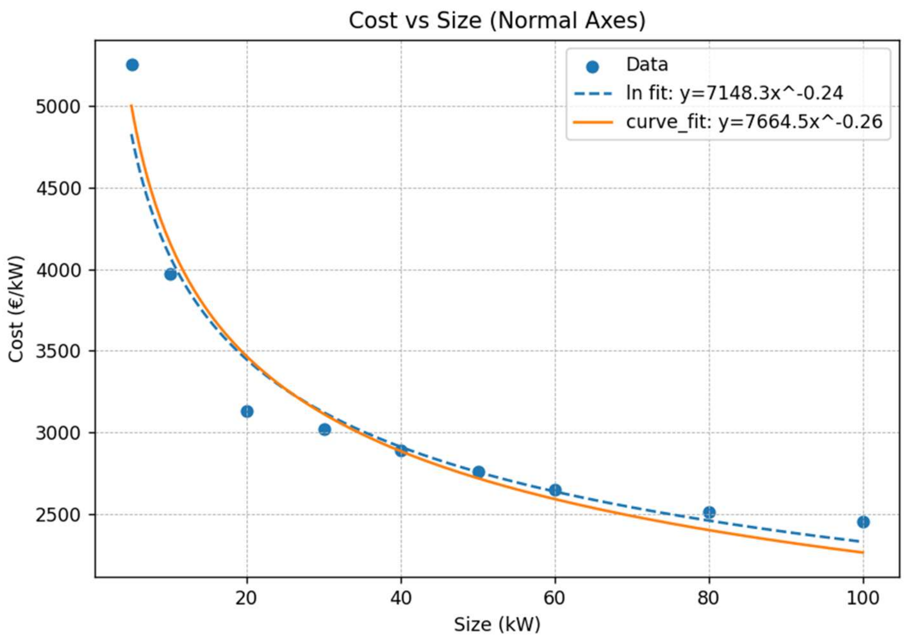

Figure B21: Analysis in linear space (correlation for geothermal heat pump with collectors, referred to heating).